CHAPTER 4

METHODOLOGY

4.1 Introduction

Speleothems are a type of cave sediment that may exist in various shapes and types. Flowstones for example form from carbonate-rich water flowing over the cave walls and floor, whereas stalagmites develop from drops of percolation water and grow upwards from the cave floor (White 2004, 2007). These deposits are generally precipitated when CO_2 is degassed from the drip water solution. Changes in the chemistry of the percolation solution and the environment within the cave also contribute to speleothem formation (*e.g.* Smith & Atkinson 1976; Baker *et al.* 1996; Harmon *et al.* 2004; White 2004, 2007; Fairchild *et al.* 2006; McDermott *et al.* 2006).

Understanding the processes associated with speleothem development is important when analyzing the isotopes (*e.g.* Hendy 1971; Harmon *et al.* 1978; Dorale *et al.* 2002; McDermott 2004; McDermott *et al.* 2006; Sundqvist *et al.* 2007; Mattey *et al.* 2008), trace elements (*e.g.* Goede & Vogel 1991; Hellstrom & McCulloch 2000; Desmarcheliar *et al.* 2006; Johnson *et al.* 2006) and growth laminations (*e.g.* Baker *et al.* 1993, 1996; Hellstrom *et al.* 2006) contained in these deposits. In palaeoenvironmental studies, these proxies are helping to identify periods and elucidate patterns of environmental change linked to precipitation (*e.g.* Johnson *et al.* 2006; Hodge *et al.* 2008; Overpeck & Cole 2008), vegetation (*e.g.* Dorale *et al.* 1998; Hopley *et al.* 2007) and temperature (*e.g.* Gascoyne 1992; Lauritzen & Lundberg 1999). In archaeological contexts, the proxies are useful in refining chronologies of human occupation (*e.g.* Schwarcz *et al.* 1980; Frumkin *et al.* 1999; Vogel 2001; Marean *et al.* 2004, 2007; Vaks *et al.* 2007) and contributing to our understanding of how past populations responded to climate change. Temporal constraint and dating of these palaeorecords is obtained using high resolution uranium series techniques.

In this study, stable carbon and oxygen isotopes were used as vegetation and climate proxies to reconstruct the environment of the region. This chapter presents the background and explains the application of the chosen methods. The first section describes in detail how speleothems form and examines the factors affecting deposition. The second part addresses the principles of U-series dating and outlines the procedure for the chemical preparation of the samples. This section also presents the method for the stable isotope analysis. A chapter summary is provided at the end.

4.2 Speleothem formation

4.2.1 Dissolution of the De Hoop limestone

The De Hoop Nature Reserve has more than a dozen limestone caves with karst topography of dolines (funnel-shaped hollows in the limestone) and poljes (circular & oval-shaped depressions) (Marker & Holmes 1999, 2005). Calcium carbonate is the main component of this limestone. During lithification when the calcium carbonate is deposited into pore-spaces between grains of sediment, the unconsolidated material is transformed into rock (Ford 1976). The coastal limestones (comprised of lithified aeolian nearshore & beach deposits) are covered by a 0.5 m thick calcrete layer (Marker & Holmes 1999, 2005). The basal limestone deposits belong to the *c.* 5.3 Ma Wankoe Formation (Marker & Holmes 2005; Holmes *et al.* 2007). The carbonates comprising these limestones are sourced from the shell debris of the overlying fossil dunes (calcarenite) and belong to the *c.* 2.5 Ma Waenhuiskrans Formation (Marker & Holmes 2005; Holmes *et al.* 2007). These geological units form part of the Bredasdorp Group sediments that overly the older Cape Supergroup sediments (Marker & Holmes 1999).

Although the De Hoop caves are formed in quartzite the limestone overlying the basal Table Mountain Group (TMG) sandstone is easily dissolved by percolating water. Dissolution occurs primarily in the presence of carbonic acid. Limestone though, is insoluble in water and the dissociation of water produces very few ions,

which can dissolve the carbonate. This interaction between water and the carbonate substrate is expressed as

$$CaCO_{3(s)} + H_2O_{(l)} \leftrightarrow Ca^{2+}_{(aq)} + HCO_3^-{}_{(aq)} + OH^-_{(aq)}$$

The CO_2 required to form carbonic acid is available from the soil atmosphere, produced during microbial decay of organic matter and released into the soil during plant respiration. During hydration, this CO_2 interacts with the water to produce carbonic acid, H_2CO_3. This reaction is expressed quantitatively as

$$CO_{2(aq)} + H_2O_{(l)} \leftrightarrow H_2CO_{3(aq)}$$

The weak corrosive action of this acid (H_2CO_3) can dissolve the $CaCO_3$-rich rock at a rate of *c.* 74mg/L of CO_2 at 10 ^oC (Smith & Atkinson 1976; Picknett *et al.* 1976). This is described by the equation below.

$$CaCO_{3(s)} + H_2CO_{3(aq)} \leftrightarrow Ca^{2+}_{(aq)} + 2HCO_3^-{}_{(aq)}$$

The H_2CO_3 also dissociates to produce HCO_3^- ions. The bicarbonate in turn, dissociates to form H^+ ions and carbonate, CO_3^{2-} as follows

$$H_2CO_{3(aq)} \leftrightarrow H+_{(aq)} + HCO_3^-{}_{(aq)}$$

Bicarbonate dissociation however, is pH dependent and occurs between pH 4.4 and 8.3 which is within the range for the waters of most limestone and dolomite environments (Ford & Williams 2007). In this range, HCO_3^- is the main form of aqueous CO_2 (Mills & Urey 1940).

During dissolution, the newly released Ca^{2+} and CO_3^{2-} ions become suspended in solution. If these ions are not removed from the surface of the carbonate rock, active dissolution stops even before the water is saturated. Consequently, the rate of dissolution depends on the rate at which $CaCO_3$ ions are transported away from the limestone surface, the speed with which Ca^{2+} and CO_3^- ions recombine and whether dissolution occurs under 'open' or 'closed' conditions (see section 4.4). This reaction is summarised as

$$CaCO_{3(s)} + H_2O_{(l)} + CO_{2(g)} \leftrightarrow Ca^{2+}_{(aq)} + 2HCO_3^-{}_{(aq)}$$

In the equation above, the forward reaction represents active dissolution and the back reaction marks the end of carbonate dissolution. It is also during limestone dissolution that calcite, which is the most ubiquitous of the cave minerals, is introduced into the sediment (White 2007).

Carbonate ions are taken into solution until there is equilibrium between the water at the CO_2 partial pressure brought down from the soil (White 2004). Upon entering an air-filled cave, this solution reaches equilibrium with the cave air by removing CO_2 from solution. This removal of CO_2 occurs because most caves are ventilated and consequently the cave atmosphere has a lower CO_2 content compared to the soil atmosphere.

Near the cave entrance evaporation is prevalent and often produces porous, rapidly precipitated speleothems which may not be suitable for stable isotope analyses (particularly $\delta\ ^{13}C$) (see section 4.6).With regard to U-series dating, samples obtained in close proximity to the cave entrance are not usually used because they are likely to be contaminated by allogenic dust containing ^{230}Th. Deeper within the cave however, humidity is typically between 95 and 100% and it is here where calcite or aragonite precipitation occurs through degassing (McDermott *et al.* 2006). During this process of degassing, the solution is supersaturated with carbonates that precipitate out to form speleothems such as stalactites, flowstone and stalagmites.

Stalactites for example form when CO_2 is degassed from the percolation water and the calcite suspended in the solution precipitates out. Over time and many drips later, the stalactite forms and grows downward from the roof of the cave. Stalagmites also form by cave drips but grow upward from the cave floor. Dripping water from the tips of active stalactites also assist with stalagmite growth. The sheet-like flowstone by contrast forms from water flowing over the cave walls. Since these speleothems form from the progressive build-up of precipitated calcite, growth laminations are deposited in such a way that younger ones overlie older layers.

4.2.2 Cave air, temperature & speleothem deposition

Generally, temperatures within the cave remain relatively constant and are often similar to the mean annual air temperature of the area above the cave (McDermott *et al.* 2006). Areas closer to the cave entrance may by contrast be more susceptible to fluctuations in temperature (Fairchild *et al.* 2006). In some

instances, these fluctuating temperatures between the cave interior and the outside can trigger corresponding changes in cave ventilation (Mattey *et al.* 2008). The chimney effect, considered the most important type of air movement within the cave system, occurs in response to this temperature difference (Wigley & Brown 1976). These temperature differences create corresponding pressure changes within the cave. This in turn, causes air to move from the cave entrance to the roof or vice versa and can result in changes in temperature and humidity (Wigley & Brown 1976).

With regards to CO_2 degassing, differences between the partial pressure of CO_2 in the drip water and the cave are also affected by the temperature (White 2004). In response to increasing temperature, carbonate solubility is typically reduced at a rate of 1.3% per ^oC (at 10 ^oC) (Smith & Atkinson 1976). Preliminary results from a recent study at New St. Michael's Cave on the Gibraltar peninsula indicate that variations in cave ventilation are particularly important in triggering CO_2 degassing. Mattey *et al.* (2008) noted a rise in cave CO_2 during winter while a reduction in the cave CO_2 was observed in summer. The lower CO_2 pressure recorded during summer coincided with comparatively more calcite supersaturation than in winter (Mattey *et al.* 2008). During the colder months, elevated cave CO_2 coincided with slower degassing and lower calcite supersaturation (Mattey *et al.* 2008).

This inverse relationship between CO_2 degassing and temperature is explained by Henry's Law. According to this law, at a constant temperature the solubility of a gas dissolved in a specific volume of liquid is directly proportional to the partial pressure of the gas (P_{gas}) above the solution (Silberberg 1996) Henry's Law is expressed as

$$S_{gas} = KH \times P_{gas},$$

Where S_{gas} is the solubility of the gas (mol/L), Pgas is the partial pressure of the gas (atm) and KH is the temperature-dependent Henry's Law constant. For CO_2 in water, KH = 3×10^{-2} mol/L.atm at a temperature of 25 ^oC (Silberberg 1996).

4.3 The De Hoop caves

4.3.1 Sample selection and the De Hoop caves

The majority of the De Hoop caves are marine abrasion caves. These caves formed by mechanical erosion along fractures in the basal quartzite of the Table Mountain Group (TMG) sandstone. The rate at which these karst forms developed was however also influenced by the local climate, underlying geology and the extent of vegetation cover above the cave. In April 2008, speleothem samples were collected from a series of caves along the coast and in the eastern end of the reserve (Fig. 4.1 a, b).

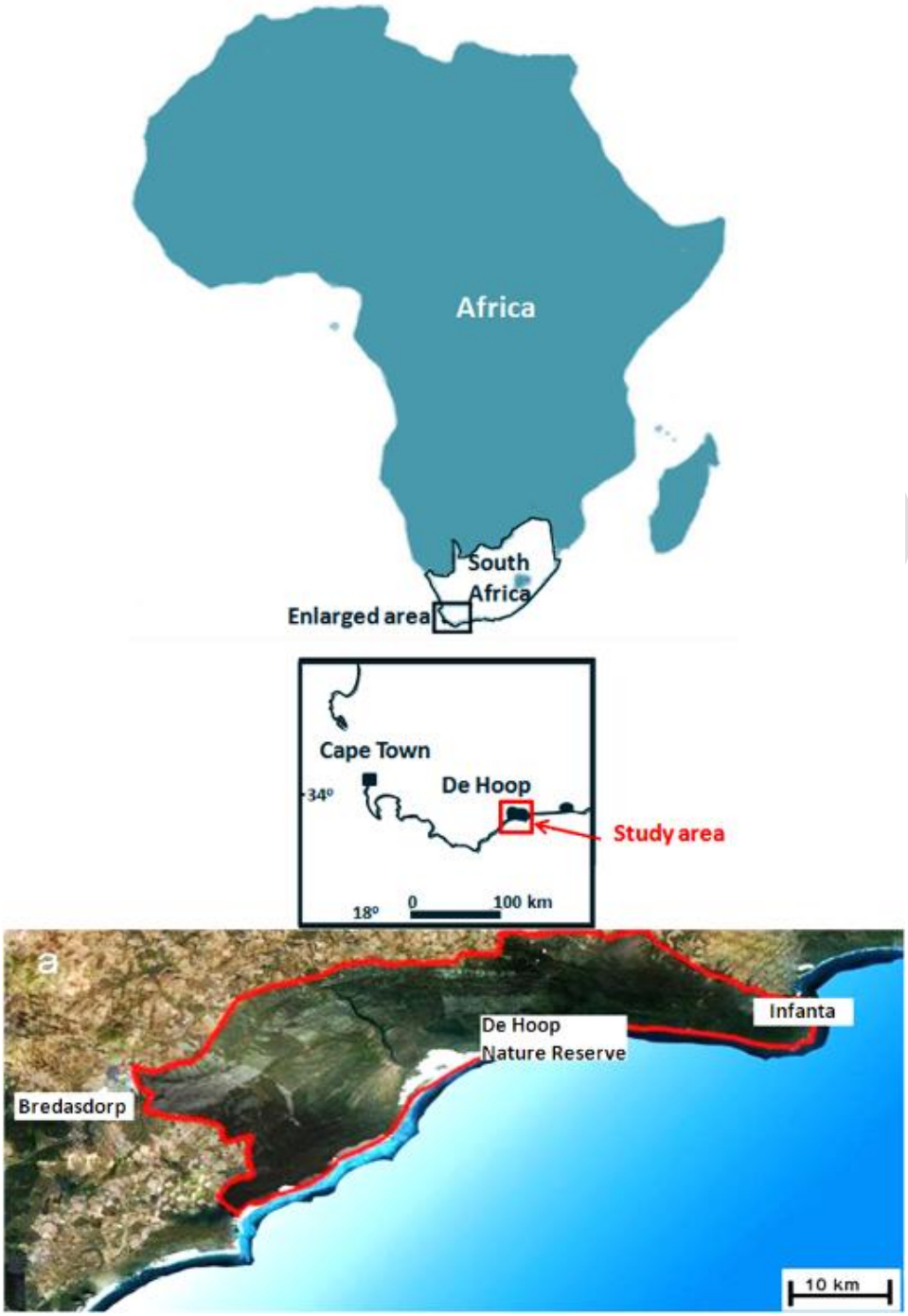

Figure 4.1 (a) Extent of the De Hoop Nature Reserve

Figure 4.1 (b) Location of the caves surveyed in the reserve during April 2008

Figure 4.2 (a & b) Box Cave (34^{o} 27.058'S, 20^{o}42.011'E)**.** (a) This is an inactive sea cave and receives light through an easily visible entrance. (b) Most of the speleothems in this cave are broken stalagmites and flowstones

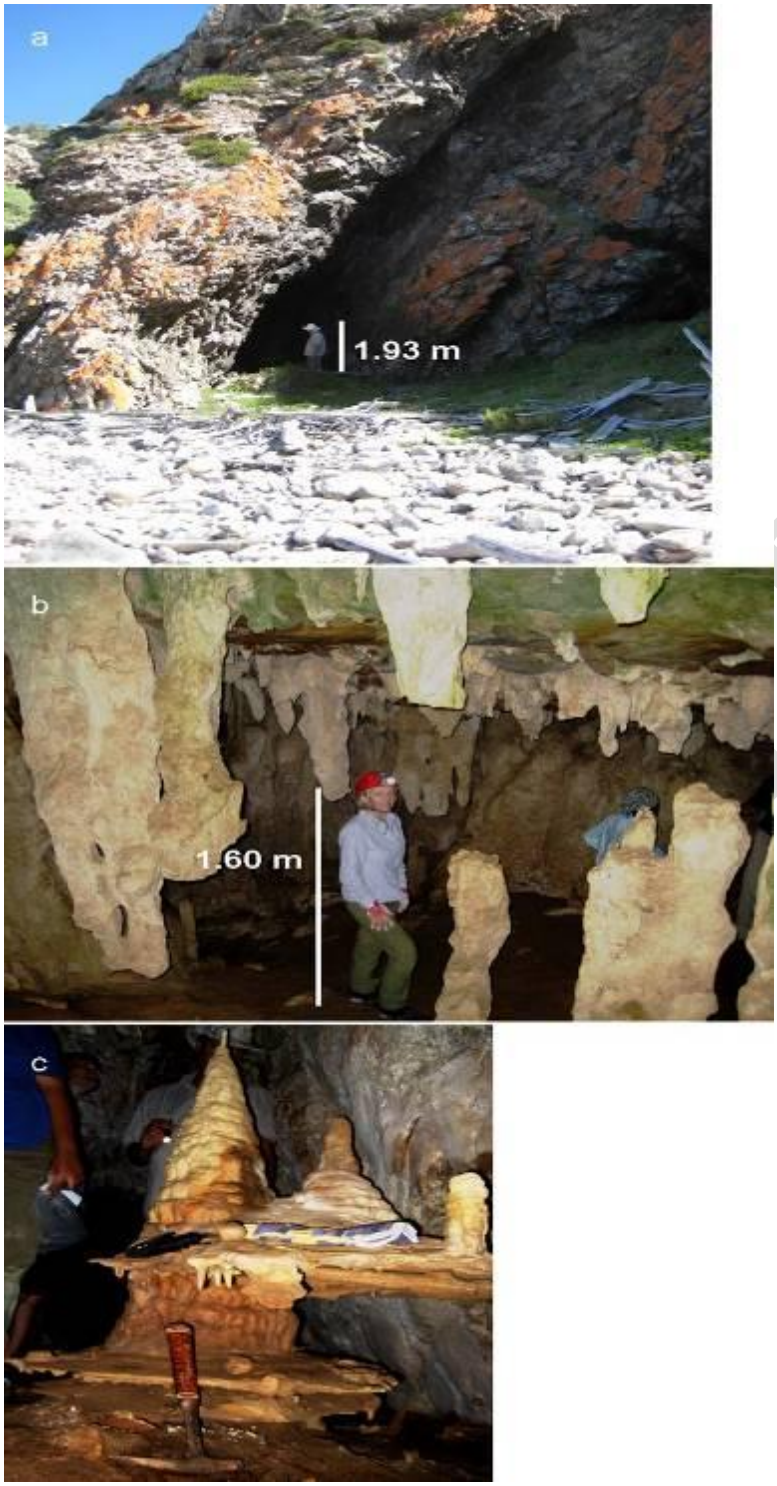

Figure 4.3 (a-c) West Cave (34°27.049'S, 20°41.883'E). (a) West Cave is some 500 m from Box Cave and comprises a prominent entrance with an unstable scree slope leading to a main chamber. Two passages branch off from the graffiti decorated chamber walls. (b) The entrance to the short, low southern passage is blocked by large, inactive, discoloured and broken stalagmites. These fossil stalagmites also line the northern passage of the cave. (c) Although there are pockets of active speleothems at both ends of passages, speleothems at West Cave are mainly fossil stalagmites and false floors

Figure 4.4 Morris's Cave (34°27.061'S, 20°42.016'E). This cave is located on an unstable scree slope. The narrow entrance leads to a wide chamber where there are a myriad of active, honey-coloured speleothem deposits. Many of the newly formed speleothems are quite fragile and are easily broken

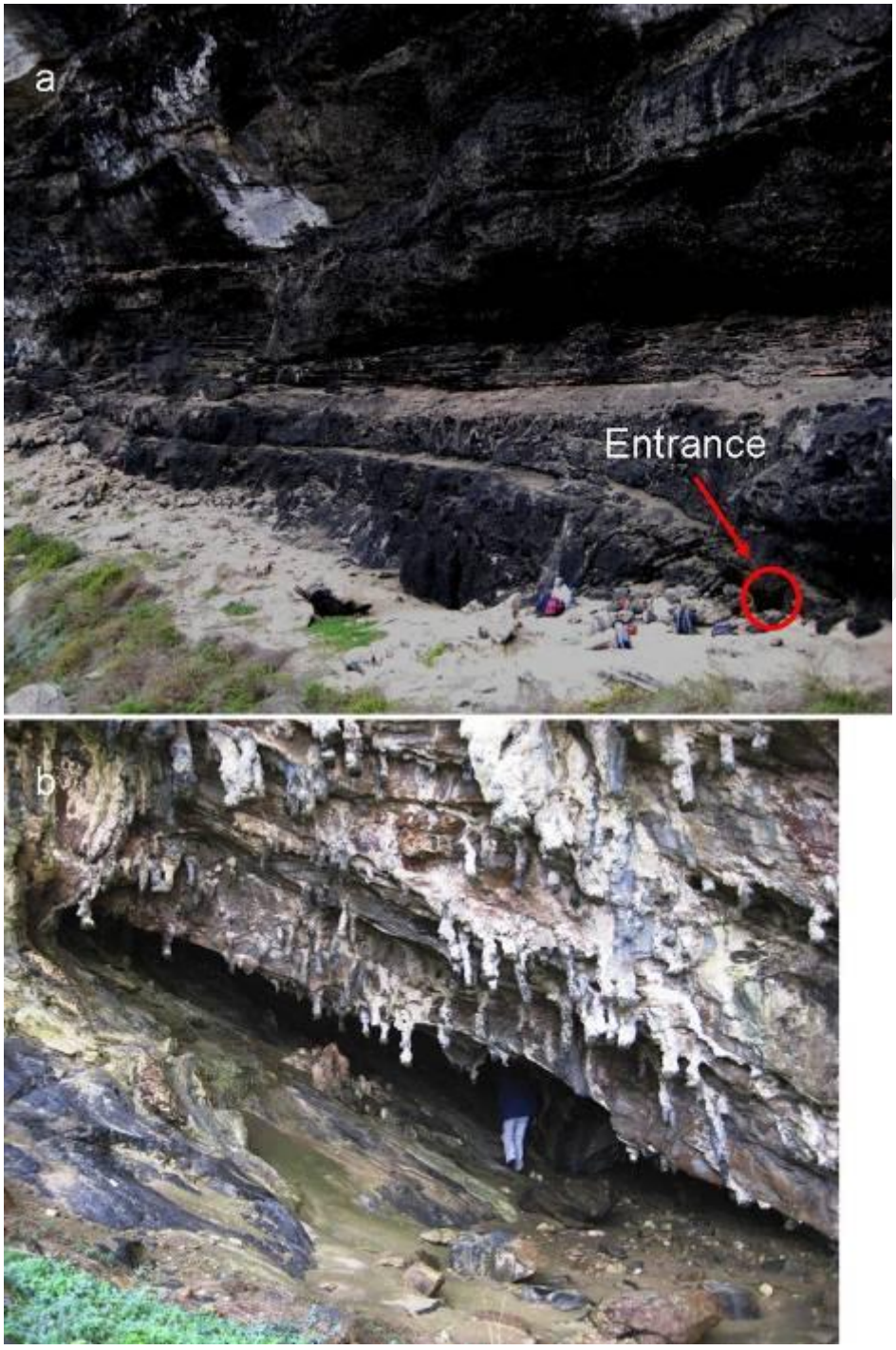

Figure 4.5 (a & b) Bloukrantz Cave (34°27.557'S, 20°46.697'E). This is an impressive sandstone cave, *c*.5 km from West Cave with an overlying limestone top from which speleothems are deposited. (a) The restricted entrance at the base of the cliff leads down an unstable earth slope to the main cavern. The walls and central area of this cavern is covered with flowstone. These speleothems are relatively clean, undamaged, active and moist. (b) There are also sandy stalactites outside the cave on the overhanging lip of the sea cliff

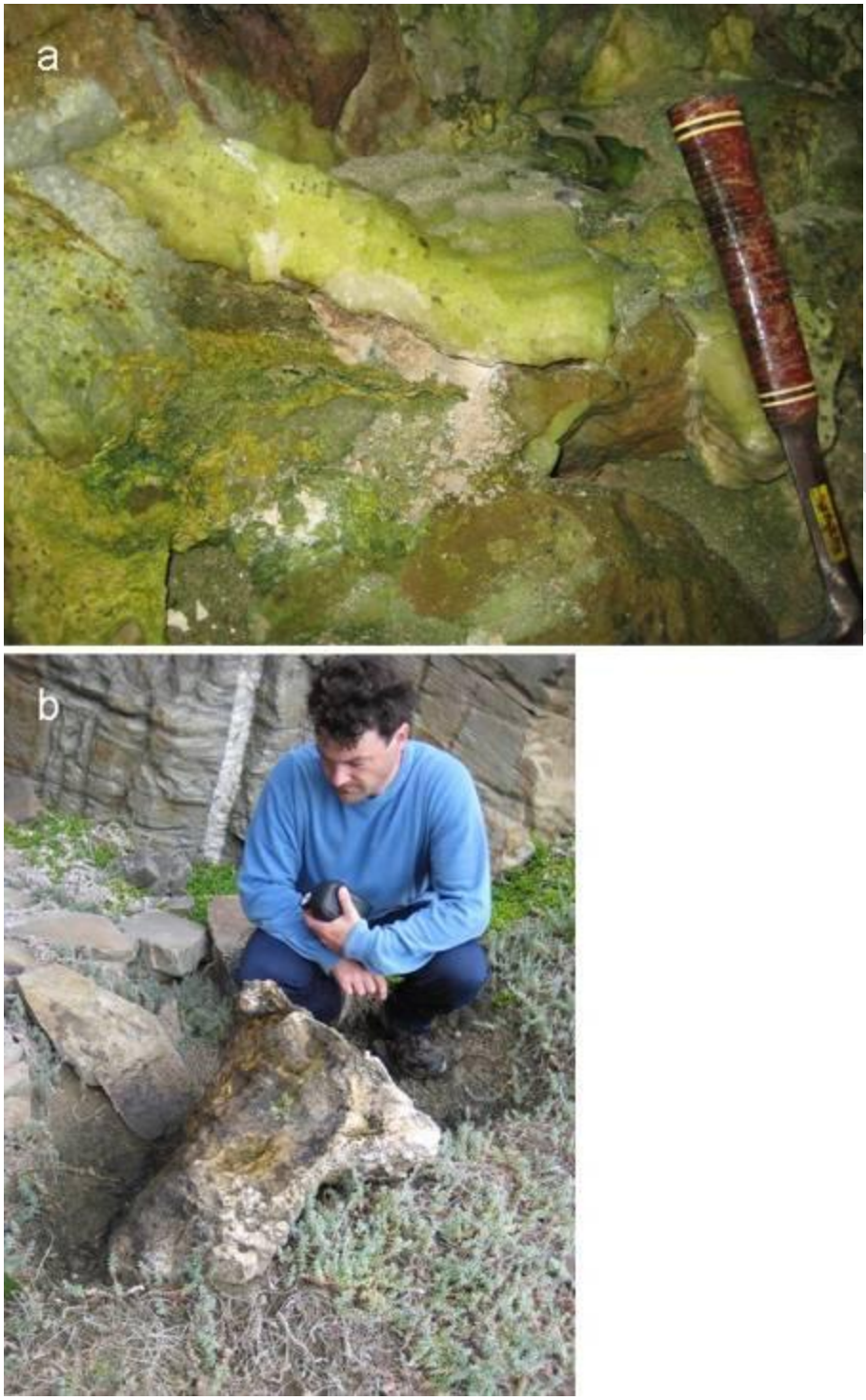

Figure 4.6 (a -c) Kaisers Gat II (34°28.248'S, 20°49.634'E). (a) Kaisers Gat II is *c*.8 km from Bloukrantz Cave and speleothems are mainly (b) flowstone and (c) fossil stalagmites

Based on a preliminary analysis the samples from Box Cave and Morris Cave were rejected because they were not suitable for U-series dating (see section

4.4.2). The Box Cave sample was rejected based on an inspection of the cave environment. This cave has a particularly large and conspicuous entrance with natural light penetrating almost to the back of the cave (see Fig. 5.2a). In addition, most of the speleothem material found in this cave is relatively weathered and brittle (Fig. 4.2b). Since ideal samples for U-series dating (discussed in section 4.4) should be relatively clean and undamaged, the Box Cave material was not used for analysis. Although the Morris' Cave speleothems come from a cave with a restricted and narrow entrance, many of the speleothems show signs of re-solution, others are quite fragile and some are hollow inside (Fig. 4.4). As a result, these speleothems were not used for experimental analysis.

The stalagmites from the Bloukrantz (Fig. 4.5), West Cave (Fig. 4.3) and Kaisers Gat II Caves (Fig. 4.6) were retained including a flowstone from Kaisers Gat II. These samples are described in more detail in the section below.

4.3.2 Brief description of the De Hoop speleothem samples

Since speleothem morphology is influenced by the environmental conditions operating inside and outside the cave, observations of the stratigraphy, growth direction and flow conditions provides some insight into the circumstances surrounding the speleothem formation (Dreybrodt 1999: 355).

This visual inspection also enables suitable samples to be selected for U-series and isotopic analysis. The samples used in this study are fossil stalagmites from Bloukrantz Cave (*Blou1*) and Kaisers Gat II (*KG2.1* & *KG2.3*) and a flowstone called *KG2.2*, also obtained in Kaisers Gat II. These caves are located within 8 km of each other and are contained within the De Hoop Nature Reserve.

Sample *Blou1* is a fossil stalagmite with a height of *c.* 150 mm and diameters of 5.5 and 7.5 mm near the top and base, respectively. Individual growth layers are visible throughout the stalagmite. These compact growth bands vary in colour from light grey (10YR 7/1) at the top to off-white (10YR 8/1) at the base. There are alternating laminations of cream (10 YR 8/2) and saddle tan (10 YR 4/4) between 2 and 7.5 mm from the top (Fig. 4.7). Changes in the growth direction

are also evident and may be indicative of variable conditions within the cave environment (possibly differences in the drip rate & available water). The deposition of aragonite over calcite minerals in the upper section of the *Blou1* stalagmite is a particularly interesting feature. This is because the deposition of aragonite is generally considered indicative of reduced drip rates and changes in the local hydrology. The presence of aragonite has palaeoclimatic significance since its deposition is associated with either drier or colder conditions above the cave (*e.g.* Frisia *et al.* 2002; Baldini *et al.* 2005; Holzkämper *et al.* 2009).

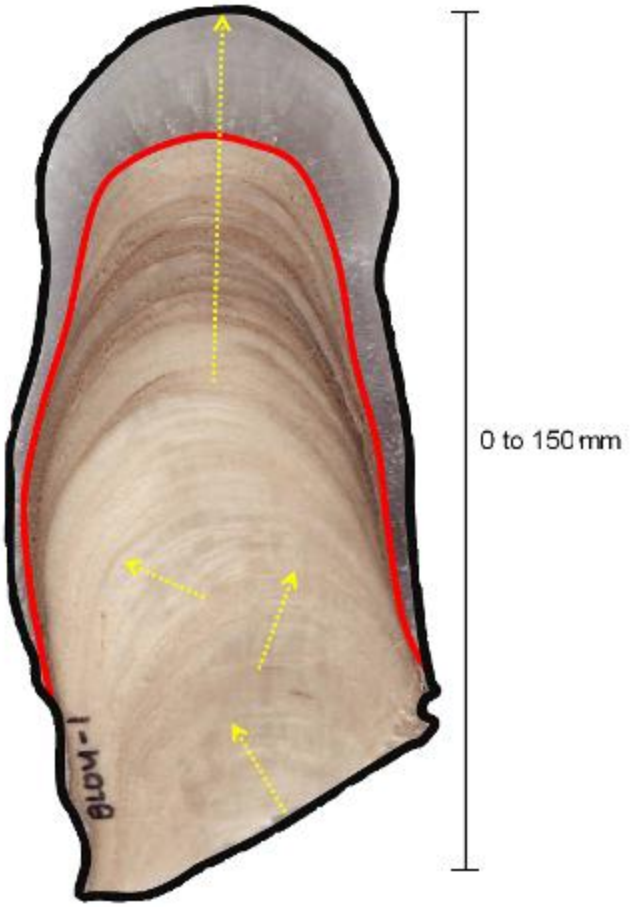

Figure 4.7 Longitudinal section through the Bloukrantz Cave sample *Blou1*. The inner line (red) represents a transitional layer where mineral deposition changed from calcite in the lower part to aragonite at the top. The presence of aragonite in speleothems is considered indicative of declining drip rates, which has in turn been related to reduced precipitation above the cave (*e.g.* Frisia *et al.* 2002; McMillan *et al.* 2005). Aragonite deposition may however also be related to changes in percolation paths associated with the local hydrology. The presence of this mineral in the *Blou1* speleothem fabric is therefore interesting since it could be indicative of drier conditions above the cave. The stippled line (yellow) indicates the changes in growth direction

The 40 mm long stalagmite, *KG2.1* has distinctive and heavy growth bands. These laminations vary in colour from light tan (10 YR 6/4) near the top to alternating bands of light brown (10 YR 5/4) and dark brown (10 YR 3/2) below the pores (Fig. 4.8). The compact layers at the top contain visible detrital material and these layers are not suitable for U-series dating. The rest of the laminations are quite dark and imply a high organic content. However, no other visible signs were noted to rule out the suitability of this sample for analysis.

Figure 4.8 Cross-section of the *KG2.1* stalagmite. The inner line (red) near the top represents a region containing substantial detrital material. Macroscopic pores are indicated by the stippled circles (yellow). These pores suggest a rapid change in calcite deposition in the middle section of the stalagmite

The single flowstone sample used in this study was represented by *KG2.2*. This 44 mm long speleothem comprises close to five visible bands alternating in colour between light grey (10 YR 7/1) and light slate grey (10 YR 6/1) with translucent calcite crystals (Fig. 4.9).

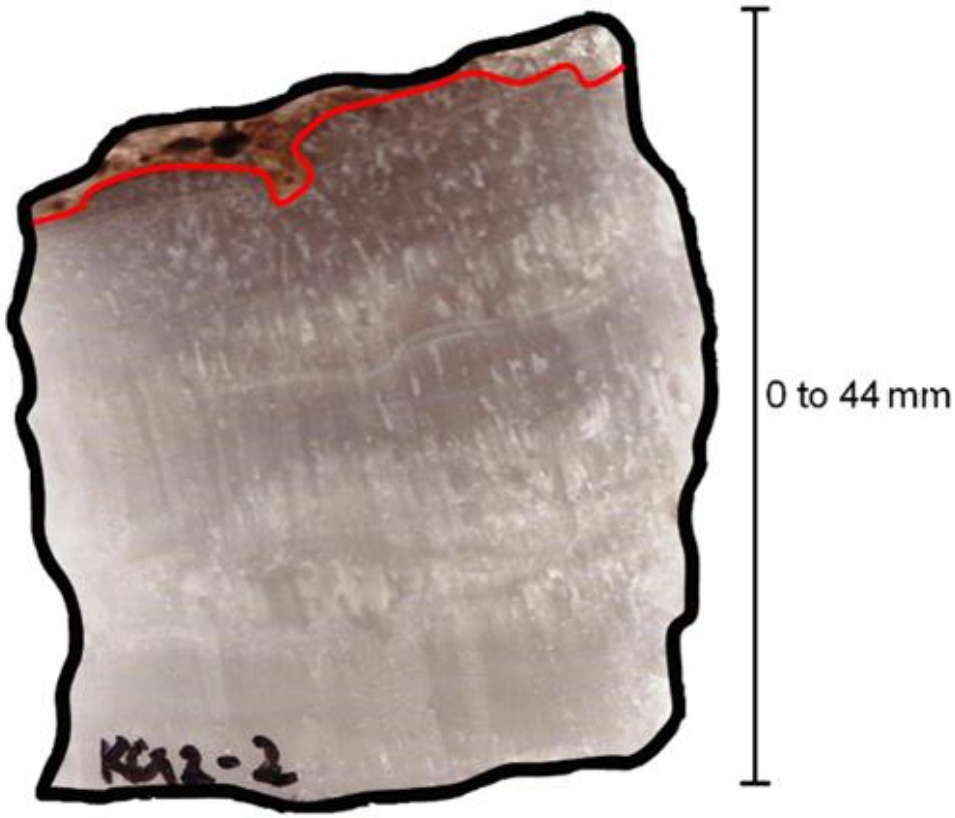

Figure 4.9 The *KG2.2* flowstone sample from Kaisers Gat II. The inner line at the top (red) represents a hard surface crust detrital material

Sample *KG2.3* is a large fossil, broomstick-shaped stalagmite *c.* 208 mm in height and 7.5 mm in diameter at the top and near the base. Since this sample is broken in both ends the top and bottom of the stalagmite was determined from the visible growth bandings. Growth laminations along the central axis are continuous and compact. The bands here alternate between dark and light brown variations from brown (10 YR 4/2) to cocoa brown (10 YR 4/3) and saddle tan (10 YR 4/4). On the extremes of the central axis the layers are visible as undulating ripples. This may be indicative of shifts in the drip rate and other factors relating to changing conditions in the cave environment. As recorded in *KG2.1*, the *KG2.3* sample also has dark laminations, which are taken as a sign of humics and other soil-derived material. Still, this sample was considered for further analysis.

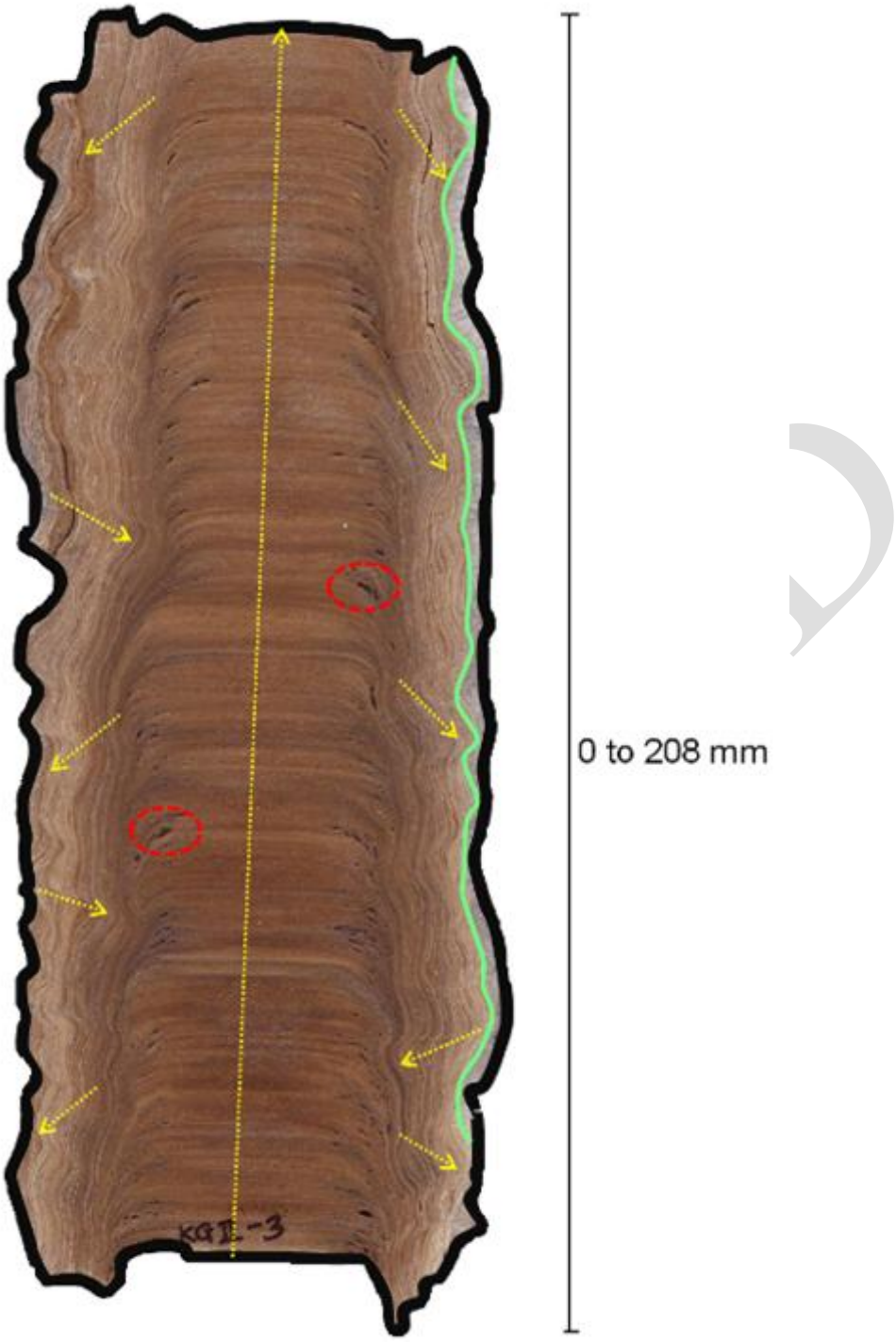

Figure 4.10 The *KG2.3* sample from Kaisers Gat II. The inner line (green) represents a region containing coarse, translucent calcite crystals. The central arrow (yellow) indicates the main growth direction while the smaller arrows on either side of the central axis correspond to rapid changes in growth direction. The stippled circles (red) relate to visible pores in the stalagmite

The stalagmite samples from West Cave and Kaisers Gat II were cast in gypsum before cutting 10 and 15 cm longitudinal sections, respectively with a rock saw on

a 3 mm thick blade. These sections were then cut into two equal halves which were used for U-series dating and isotopic analyses, respectively.

4.4 Uranium series dating

4.4.1 Principles of uranium series dating

The number of protons determines the atomic number of an element whereas the mass is the sum of the protons and neutrons in the atom. It is the number of protons that determines the type of element. This in turn, determines the number of valence electrons that surrounds the nucleus. The electron configuration gives an element its chemical properties.

Isotopes are forms of a chemical element with the same number of protons and electrons but different numbers of neutrons in the nucleus of the atom. They are consequently identical chemical elements but with a different atomic mass.

$$_{Z}{}^{A}X_{N}$$

Where X is the element, A represents the atomic mass, Z is the atomic number and N is the neutron number.

Uranium has three isotopes, ^{234}U, ^{238}U and ^{235}U and its daughter isotopes, ^{234}U, ^{230}Th (thorium)and ^{231}Pa (protactinium) which is used for dating (Schwarcz 1992; Smart 1991). The timescale for uranium series dating covers an age range up to 1.5 Ma (Smart 1991; White 2004). U-series dating is based on the decay of a parent isotope to a daughter isotope where the decay rate of an isotope is determined by its half-life. The half-life is the time taken for half of the original atoms of an isotope to decay and can be calculated as follows:

$$t\,½ = \ln 2/\lambda$$

Each decay event produces a single daughter isotope and the relationship between the half-life and decay constant is given by:

$$N_t = N_o e^{-\lambda t}$$

Where, N is the number of parent atoms, t represents time, N_o is the original number of atoms at time zero and $e^{-\lambda t}$ is the decay constant.

If a nucleus contains an excess of neutrons or protons, it will eventually disintegrate to form a stable nucleus. This is known as radioactive decay; a

random process during which an isotope of one element is transformed into another element or isotope (Rink 2001).

In nature, uranium (U) has two main decay series, ^{238}U and ^{235}U with half-lives of 4.49×10^9 and 7.13×10^8 years respectively (Smart 1991; Fig. 4.11). The most plentiful isotope of thorium (Th) is ^{232}Th with an extremely long half-life of 1.39×10^{10} years. This thorium isotope is a daughter of ^{236}U with a half-life of 2.4×10^7 years. However, uranium in the form of ^{236}U (as well as ^{223}U & ^{229}Th) does not exist in nature anymore. Thorium in the form of ^{232}Th does not form part of the uranium decay series but is useful for monitoring thorium contamination.

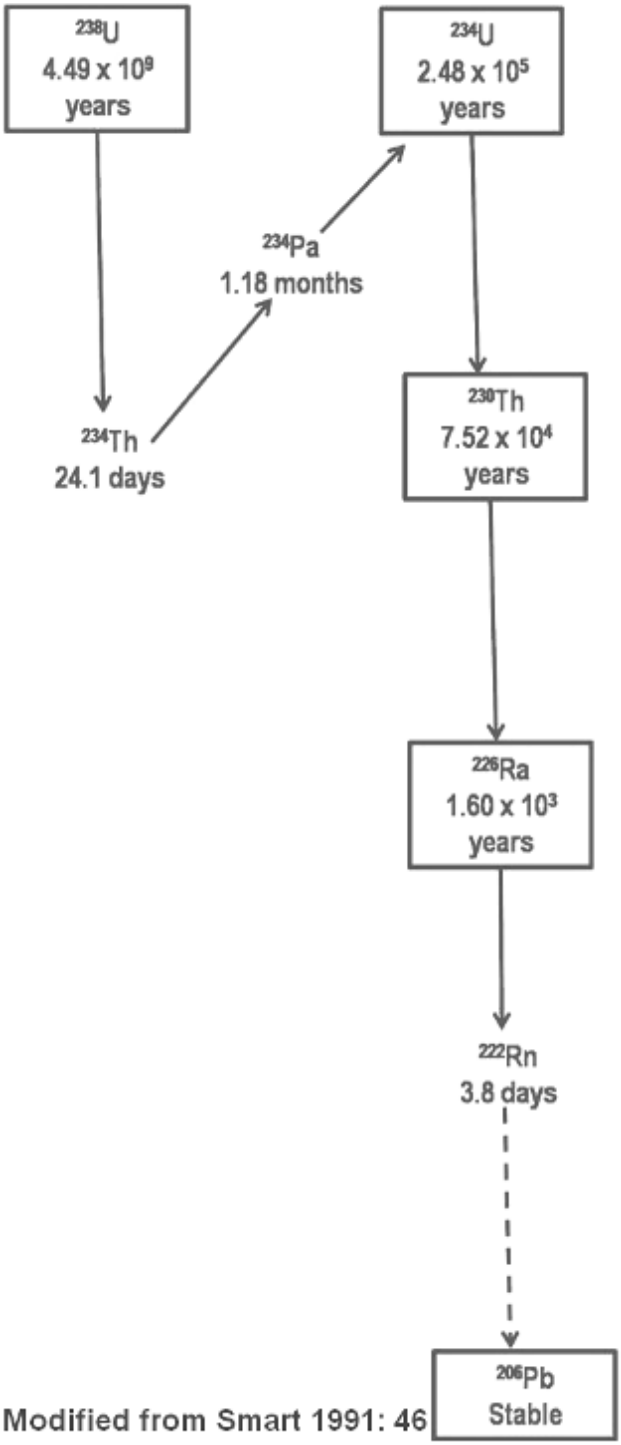

Figure 4.11 Radioactive decay series for ^{238}U including the half-lives for the long-lived isotopes; ^{238}U, ^{234}U and ^{230}Th

^{234}U is a daughter isotope of ^{238}U and has a half-life of 2.48 x 10^5 years. In the ^{238}U decay series, ^{238}U emits an alpha (α) particle to form ^{234}Th. During the alpha emission, the U atom loses 4 nucleons (as 2 protons and 2 neutrons). This loss

changes the mass number and atomic numbers of the atom, by four and two, respectively and as a result uranium is transformed into thorium.

The ^{234}Th isotope is also unstable but undergoes beta decay to form ^{234}Pa (protactinium) by emitting a beta particle. During beta (β) decay, a neutron is converted into a proton with the loss of an electron and antineutrino.

$$n \rightarrow p + e^{-} + \overline{\nu}$$

Beta decay occurs also when a proton is converted into a neutron with the emission of a positron (positive electron) and a neutrino (neutral particle).

$$p \rightarrow n + e^{-} + \nu$$

In turn, ^{234}Pa decays to form the ^{234}U isotope by emitting a beta particle. The newly formed ^{234}U then decays by alpha emission to form ^{230}Th. The ^{230}Th undergoes alpha emission to form ^{226}Ra (radium). The ^{226}Ra isotope undergoes four successive alpha and beta decays before forming the stable end product of ^{206}Pb (lead).

For U-series dating of Quaternary deposits, three daughter/parent isotope pairs are used; ^{234}U/^{238}U, ^{230}Th/^{234}U and ^{231}Pa/^{235}U. The two types of U-series disequilibrium methods - excess and deficient- are based on the concentration of daughter isotopes. The ^{230}Th/^{234}U daughter deficient method with an age range up to 500 ka is the most important one used for speleothem, bone and shell deposits (Smart 1991). The main principle behind the ^{230}Th/^{234}U method is that uranium is readily incorporated into the carbonate lattice of the material whereas thorium is hydrolyzed and adsorbed onto clay minerals and hydroxides (Langmuir & Herman 1980; Smart 1991). As a result, thorium is absent at the time of deposition and progressively increases through time.

4.4.2 Criteria for U-series dating

U-series dating assumes that:

- the decay coefficients and the initial parent/daughter ratio are known,
- during U-series analysis, radioactive decay is exclusively responsible for temporal changes in the ratio of parent to daughter isotopes (Gascoyne

1992; Smart 1991).(In the case of the $^{230}Th/^{234}U$ disequilibrium method, when the sample is deposited there should be no ^{230}Th.)

- sufficient U ($\leq$ 0.01 ppm to > 300 ppm) is present in the sample (this helps reduce possible analytical interference) (Gascoyne 1992; Ford & Williams 2007)

Any deviation from these criteria has serious implications for the reliability of age estimates. Fortunately, there are various procedures, which can be used to correct this. For example, dating clean speleothem samples without any detrital content and evidence of re-crystallization. Subsample selection is therefore important for a reliable result.

With regards to the $^{230}Th/^{234}U$ isotopic ratio, thorium contamination is evaluated from the ^{232}Th concentration within a sample (Smart 1991; Schwarcz 1992). The ^{232}Th content is obtained from the $^{230}Th/^{232}Th$ and $^{232}Th/^{238}U$ ratios (Dorale *et al.* 2004). Contamination is caused when ^{230}Th is incorporated into the crystal lattice of carbonate or aragonite structures. During the incorporation of ^{230}Th, ^{232}Th is also taken up. In general, ^{230}Th is corrected for when the $^{230}Th/^{232}Th$ ratio is less than 20 (Smart 1991). However, for the inductively coupled plasma mass spectrometry (ICP MS) technique on which this study is based the ^{230}Th threshold is automatically set to 50.

Isochron techniques are often used to calculate a corrected age for samples that are contaminated by non-authigenic ^{230}Th (Ivanovich 1982; Dorale *et al.* 2004). The premise for the U/Th isochron method is that the age and isotopic composition of uranium and thorium species in the sample can be calculated from subsamples of the material (Hellstrom 2006). This method assumes that Th contamination within a single sample is homogenous. Possible contamination in the sample is then evaluated at the time of measurement using at least four analyses for each isochron. This is achieved by plotting each measurement for $^{230}Th/^{232}Th$ against the measurements for $^{234}U/^{232}Th$. These ratios are measured on the mass spectrometer and are obtained for a set of subsamples. These subsamples are usually taken from regions along the growth bands where there are obvious differences in detrital content (Dorale *et al.* 2004). Subsample measurements may

include only three data points plotted on the X-Y plot. A least squares linear regression (or some other regression approach) is applied to the data to assess the correlation between the points (Fig. 4.12). The corrected age is calculated from the slope of the line. The initial isotope ratios are then calculated from the intercept of the isochron line at the y-axis (Dorale *et al.* 2004).

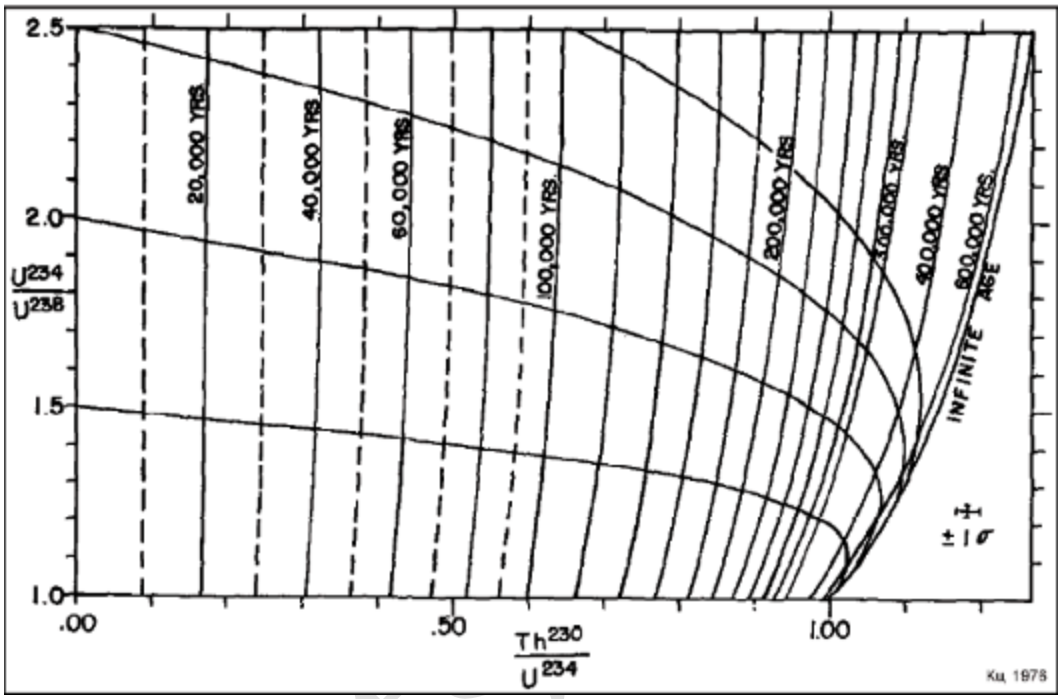

Figure 4.12 An example of an isochron plot. The age is calculated at the intersection between the vertical and horizontal lines. The 1σ error is determined by combining the error for the $^{234}U/^{238}U$ and $^{230}Th/^{234}U$ activity ratios (Ku 1976; Ivanovich 1982)

Evaluating the Th contamination is an important consideration because any introduced thorium can affect the $^{230}Th/^{234}U$ activity ratio by increasing the U-series ages (Goede & Vogel 1991). The effects of the initial Th concentration on the age estimate may be reduced with increasing U concentration, increasing age and decreasing detrital contamination (Dorale *et al.* 2004: 177).
Generally, the age of the speleothem is calculated by measuring the activity ratios of ^{234}U, ^{238}U and ^{230}Th using the equation shown below:

$$(^{230}Th/^{238}U)_A = 1- e-\lambda_{230}t (1 – (^{230}Th/^{238}U)_A (^{230}Th/^{238}U)_{Ao}) + ((^{234}U/^{238}U)_A -1)$$
$$(\lambda_{230}/(\lambda_{230} – \lambda_{234})) \times (1 – e – (\lambda_{230}- \lambda_{234})t)$$

An alternative form of this equation measures the $^{230}Th/^{234}U$ activity ratio for age calculations. Ages determined from the $^{230}Th/^{234}U$ and $^{230}Th/^{238}U$ activity ratios are not significantly different and the choice of which ratio to measure is usually a matter of preference.

The equation described above accounts for Th contamination during deposition using the $^{230}Th/^{232}Th$ ratio. $(^{230}Th/^{232}Th)_{Ao}$ is the assumed activity ratio at the time of sample deposition, $(^{232}Th/^{238}U)_A$ is the measured $^{232}Th/^{238}U$ activity ratio and λ is the isotope specific decay constant. Conventionally, initial Th is corrected for using the difference between detrital Th and measured Th (Hellstrom 2006).

In this study, corrected ages were calculated using the Age4U2U program developed by Lauritzen (1995-2007). The program is based on the ^{238}U decay series and uses the measured $^{230}Th/^{234}U$ activity ratios and an assumed $^{230}Th/^{232}Th$ activity ratio of 1.5 for age determinations. The $^{230}Th/^{232}Th$ activity ratio is referred to as the 'earth mean' which is conventionally used to account for detrital content (*e.g.* Schwarcz *et al.* 1980).

The $^{230}Th/^{234}U$ activity ratio, however, is obtained from two different sources; thorium-230 from $^{230}Th/^{232}Th$ and uranium-234 from the $^{234}U/^{238}U$ ratio. Before this ratio can be used for age determinations, it has to be corrected as follows:

$$(^{230}Th/^{234}U)_{Corrected} = (^{230}Th/^{234}U)_M \, (^{232}U/^{228}Th)_M \, (^{228}Th/^{232}U)_M$$

This correction accounts for variations in the concentration of Th and U and differences the chemical yield of ^{234}U, ^{238}U and ^{230}Th. These corrected ratios for $^{234}U/^{238}U$ and $^{230}Th/^{234}U$ are then used for age determinations in calendar years.

4.5 Chemical preparation of the De Hoop samples for U-series dating

4.5.1 Sampling approach for U-series dating

In U-series dating, daughter isotopes may be measured using a range of mass spectrometry techniques - alpha-particle spectrometry, thermal ionization mass spectrometry (TIMS), gamma-ray counting and inductively-coupled plasma mass spectrometry (ICP MS). In this study, uranium and thorium activity ratios were

measured using the inductively coupled plasma mass spectrometry (ICP MS) technique adopted from Hellstrom (2003).

Prior to analysis, the samples were pre-treated at the Geosciences Institute of the University of Bergen. Subsamples (*c.* 5-10 mm thick) were taken along the length of stalagmite and flowstone material using a dentist drill with a 0.5 mm burr tip. These samples were then weighed on an analytical balance. Organic residues were removed from samples by incinerating in a high purity quartz crucible at 600 ^{o}C for at least 4 hours (preferably between 6 & 12 hours). 1 ml of distilled water was added to each sample to initiate the reaction and the samples were then dissolved in a minimum amount of 14 M (concentrated) HNO_3. The amount of acid added was monitored by counting the number of drops, assuming that 20 drops approximates 1 ml.

Between 50 and 100-µl uranium spike was added to each sample using a micropipette. The amount of spike added is dependent on the spike concentration and needs to be adjusted accordingly to ensure that the sample is not over spiked. (Over spiking can only be detected during ICP MS analysis if the atomic ratio of $^{236}U > ^{235}U$. Consequently, this has to be corrected for when calculating the age). The samples were weighed, loaded into a bench top centrifuge and spun for 5 min at 2000 rpm. After centrifugation, the samples were evaporated to almost dryness and dissolved in 1 M HNO_3 to make *c.* 10 ml.

The Eichron TRU resin columns used for the ion-exchange chromatography (*i.e.*to elute uranium from the sample material) were prepared from 3 ml plastic dropping pipettes (Fig. 4.13). The bulb tips of each of the pipettes were cut off and a 0.5 mm round, porous polythene pad (Frit) positioned into each of the columns. Distilled water was then added to the empty columns and any air bubbles were gently squeezed out.

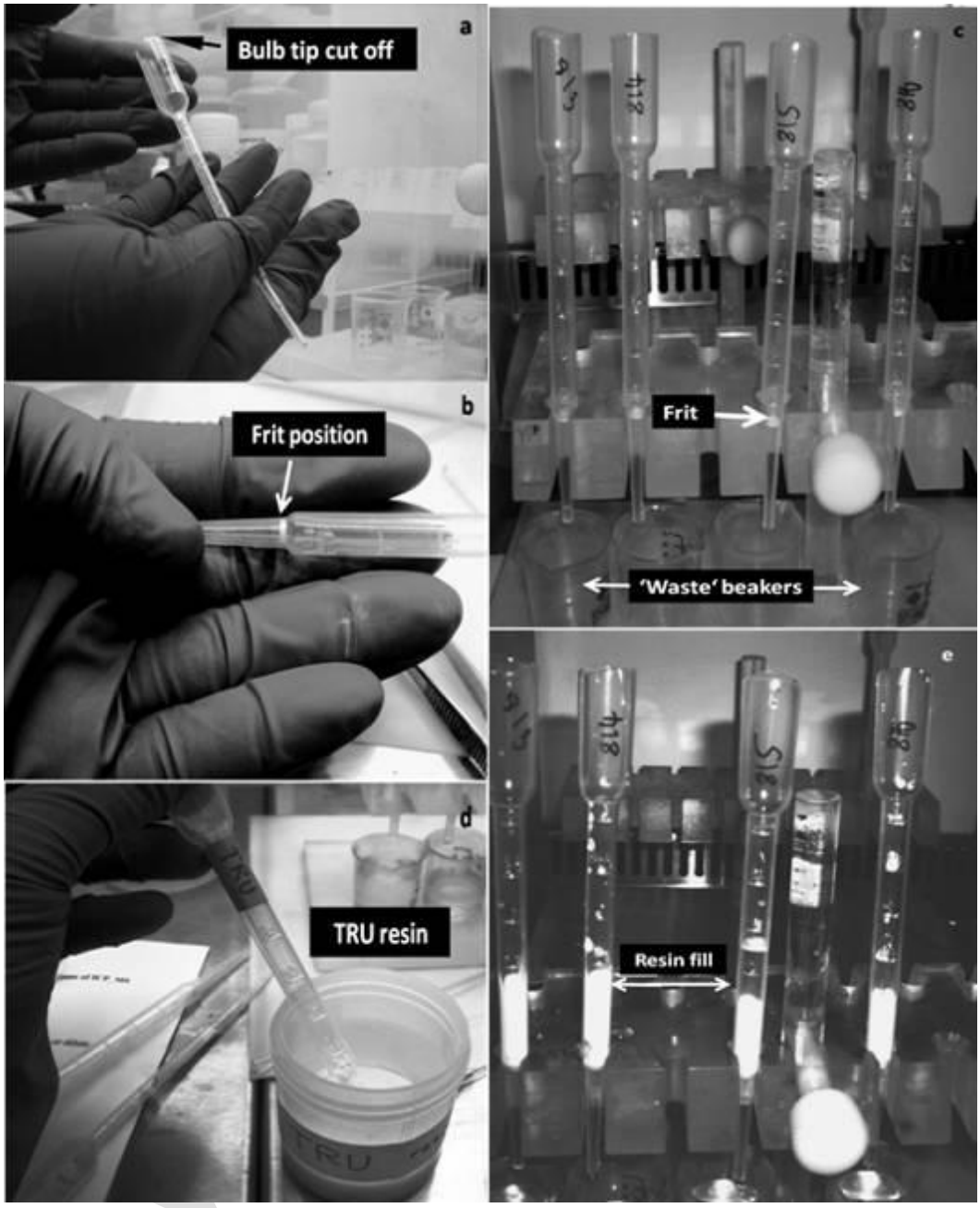

Figure 4.13 (a-e) Eichron TRU resin column preparations for U and Th elution

The total volume of resin fill was 1 ml. This is the column volume (CV) unit referred to in the rest of the procedure. One column volume (CV) of Eichron TRU-resin with particle size 100-150 µm was added to each water-filled column. (Resin of this size works at 1 M HNO_3 and therefore it is important that the HNO_3 concentration is correct). The columns were then washed with 2 CV distilled water. (2 x 2) CV 0.1 M HCl/0.2 M HF were added to remove any actinides and

clean the column for U/Th treatment, finally the column was conditioned with (1 CV + 2 CV) of 1 M HNO3.

During the sample separation step, the sample was added to the column and left to drain almost to the surface of the resin. Any remaining sample such as calcium salts was washed out with (1CV + 2CV) 1M HNO_3. Finally, (1 + 1 CV) 1M HCl was added to change the column from HNO_3 to HCl. At this stage, the column was washed free from calcium salts, but the actinides (*i.e.* uranium & thorium) were still absorbed.

Uranium and thorium were eluted from the column by adding (1 + 2 + 2) CV 0.1M HCl/ 0.2 M HF. A single drop of 14 M HNO_3 was then added to the eluate. The eluate was evaporated to dryness with little or no residue. (The ICP MS instrument cannot take salt solutions and if there is visible residue the total dissolved solids (TDS) should be < 100 mmol/l). After this stage, the samples were ready for ICP MS analysis. Using the selection criteria described in 5.4.2 a total of 15[1] samples with an average U content of 0.28 ppm were analyzed. These samples represent speleothems from Bloukrantz Cave, Kaisers Gat II (*KG2.2* & *KG2.3*).

The uranium content of the sample was calculated as the difference between the initial amount of ^{236}U which was added to the sample in the form of the spike (containing ^{236}U, ^{233}U & ^{229}Th) and the measured ^{236}U. Although it is assumed that the Th and U isotopic ratios remain unchanged during elution, uranium may be lost at some stage during the analysis. This loss therefore needs to be accounted for when determining the sample age.

4.5.2 ICP MS analyses

ICP MS analyses were conducted at the Geology Department of the University of Oslo in Blindern on a Nu Plasma High Resolution Multi-Collector ICP Mass Spectrometer. The main components of the ICP MS are the sample introduction system, ICP torch, interface, vacuum system, mass spectrometer and detector (Fig. 4.14).

1

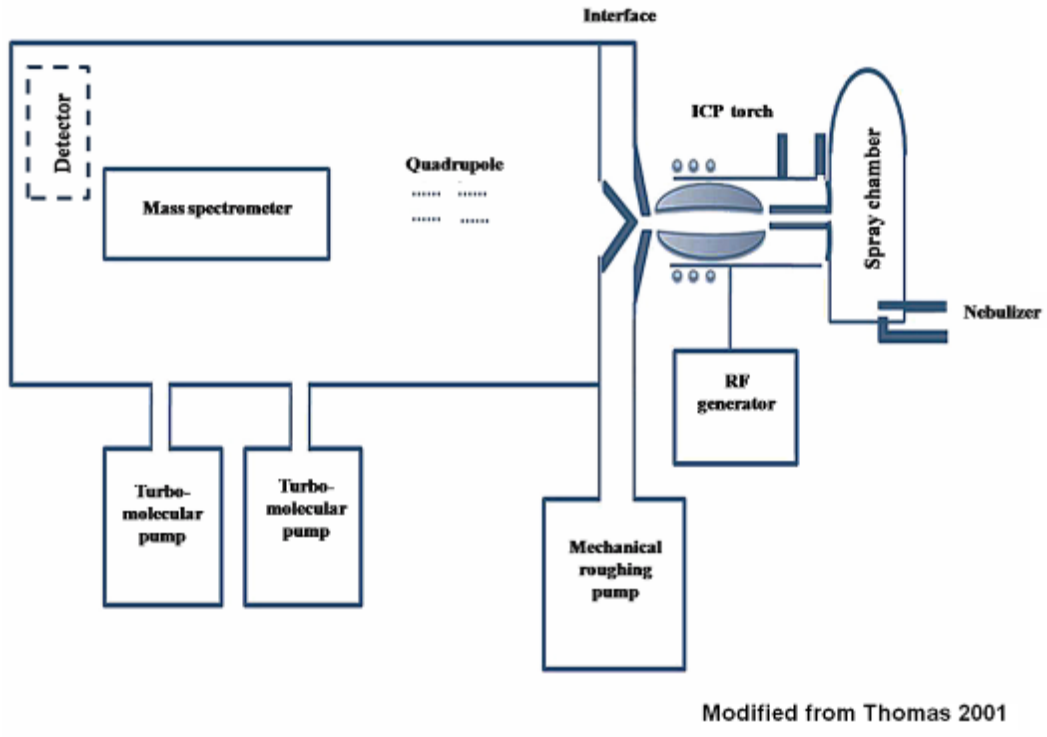

Figure 4.14 Diagram illustrating the main components of the ICP MS

The MC ICP MS at the University of Oslo handles liquid samples, which enter the machine through the nebulizer and spray chamber at the sample introduction system. The nebulizer converts the liquid samples into very small droplets which are carried via the spray chamber into the sample injector tube of the ICP torch. The torch consists of three concentric quartz tubes and argon gas is fed through the outer and middle tubes at a rate of 13 litres per minute. Argon gas is used primarily because compared to the other elements it has a high first ionization energy which ensures maximum collision rate efficiency (Amman 2007). This ensures that the sample is ionized long enough to be detected by the mass spectrometer. A radiofrequency coil operating at 40 MHz is connected to the torch through a generator, which supplies the torch with 1300 MW of power. The current passing through the coil creates an electromagnetic field in the torch and

[1] Four samples representing a stalagmite from Kaisers Gat II (*KG2*.1) were also prepared for U-series dating. However, at the time of this writing, the data was not available and is therefore not included in the total.

as the argon gas is passed through the torch it becomes ionized through the following reaction, $Ar_{(g)} \rightarrow Ar^{+} + e^{-}$

As more of the argon gas is converted into Ar ions and electrons plasma is produced. The temperatures within the torch are in excess of 6000 ^{o}C and maintained by the generator and plasma. The sample aerosol enters the plasma in the presence of nebulizer gas flowing at a rate of 0.8 litres per minute. Heating the sample to 7000 ^{o}C removes water molecules and dries it to a solid. As it moves through the plasma, further heating transforms the solid sample into a gas. At approximately 6000 ^{o}C, it is converted into a ground-state (neutral) atom. The neutral atom subsequently travels through the plasma, collides with energized argon atoms and absorbs energy from the plasma to become ionized by releasing an electron. These newly formed, singly charged ions eventually leave the plasma and move via the interface region to the mass spectrometer. This process is illustrated below:

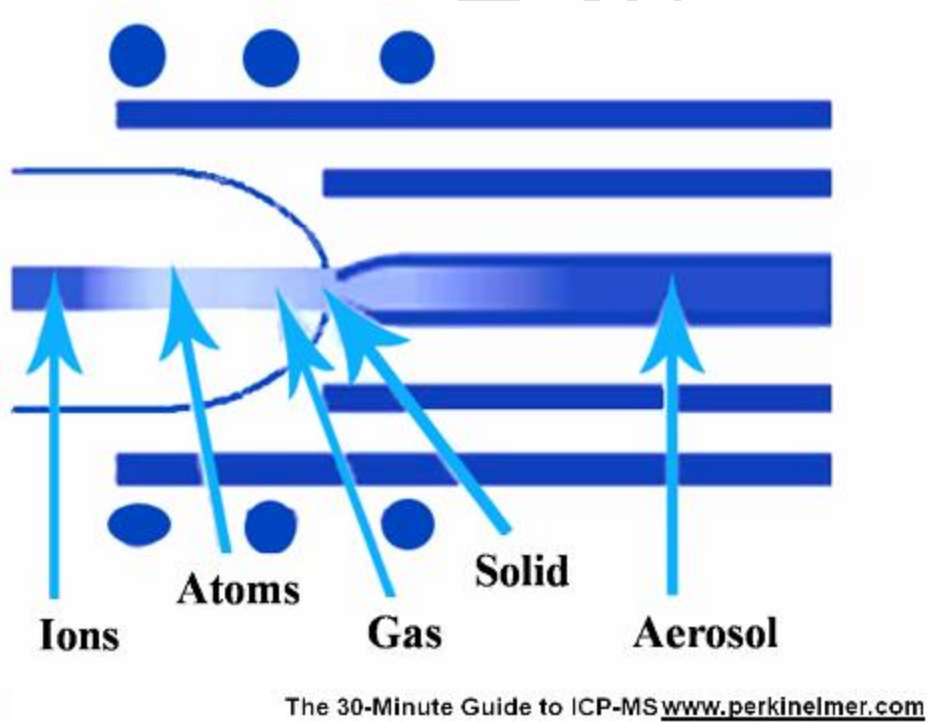

Figure 4.15 Transformation of the liquid sample as it moves from the nebulizer through the plasma, leaving the ICP torch via the interface region en route to the mass spectrometer. At the nebulizer, the sample is converted to an aerosol. As the aerosol travels through the plasma produced in the ICP torch, it is dried to a solid

and further heating changes it into a gas. In this form the sample interacts with energized argon atoms and become ionised upon leaving the ICP torch

The interface is particularly important because it connects the ICP torch and mass spectrometer. Consequently, the interface is essential in helping the ions formed in the plasma to move into the mass spectrometer. The interface has two cones and a vacuum, which help in this respect. The cones have a diameter of 1 mm, are located next to the plasma in a heat-protective, water-cooled block and are divided into skimmer and sampler types (Thomas 2001). The size of the cones helps prevent it from being blocked by foreign particles. The vacuum is created by a mechanical roughing pump connected at the interface in the space between the cones. This vacuum is maintained at a pressure of *c.*1 mbar. Another vacuum system operating between the quadrupole mass filter and detector helps maintain the pressure between these two components. The turbomolecular pumps of this vacuum, coupled with the roughing pumps at the interface ensure that ions travelling the distance (typically < 1 m) from the interface to detector do not interact with any other gas molecules en route. The ions measured at the detector were analysed using the Nu Plasma operating software.

Although the precision of the MC ICP MS is approximately 1 ‰ for $^{234}U/^{238}U$, $^{230}Th/^{238}U$ and $^{230}Th/^{232}Th$, isotope ratios have to be corrected for mass fractionation, which is linked to the interface region and collectors (Goldstein & Stirling 2003; Halliday *et al.* 1995; Heumann *et al.* 1998; Luo *et al.*1997; Pietruszka *et al.* 2002). With ICP MS, mass bias can occur during ionization and detection (Goldstein & Stirling 2003). At the interface region, mass fractionation occurs when there is an uneven transfer of ions from the skimmer cone to the mass spectrometer (Heumann *et al.* 1998). This is linked to more of the lighter ions being repelled compared to the heavier ions. As a result, mass bias is larger for elements (isotopes) with low mass numbers compared to ones with higher mass, such as U and Th (Heumann *et al.* 1998). This principle is represented by the equation below:

$$f_{MD} = R_{true}/R_{measured}$$

Where f_{MD} is the mass discrimination factor and R is the isotope ratio. From this expression the mass discrimination, MD, per mass unit per centimeter can be calculated.

$$MD = (100\ (f_{MD} - 1)\ /\Delta\ m)\ (\%)$$

For the U-Th isotopes the multi collector ICP MS has a typical mass bias from 0.5- 1% per atomic mass unit (amu) (Goldstein & Stirling 2003). This mass fractionation which occurs during detection is taken into account by adjusting the isotope ratios for the effects of drift and gain. 'Drift' refers to a disparity between known and observed isotope values for a laboratory standard used during a run, whereas 'gain' relates to variations in the efficiency of the ion collectors and Faradays (Pietruszka *et al.* 2002). In ICP MS analysis, the gain between ion counter (Daly) and Faraday cup usually varies less than 0.5% within a 45-min period (Luo *et al.* 1997). The drift in the relative gain between the ion counter and Faraday cup can be estimated in two ways. The first approach, known as a static procedure (Luo *et al.* 1997), uses the mass fractionation measured for a standard to correct for mass bias in the sample (Goldstein & Stirling 2003).In this study, the multi-static procedure was used as an alternative.

This procedure uses the instrumental mass bias for one element (*e.g.* U) to correct for fractionation in the other (*e.g.* Th) (Goldstein & Stirling 2003; Halliday *et al.* 1995). The basis for this is that ICP MS allows Th and U to be measured from the same sample in a combined U-Th run. With both methods the measured $^{238}U/^{235}U$ ratios are corrected to the natural U value of 137.98 amu (Heumann *et al.* 1998; Luo *et al.* 1997; Pietruszka *et al.* 2002). In this study, instrumental mass fractionation was corrected for relative to natural $^{238}U/^{235}U$ using $^{235}U/^{234}U$ (Pietruszka *et al.* 2002). Ninety U-Th ratios were collected within 1 hr for a single sample with the relative gain between the electron multipliers (IC_0 & IC_1) and Faraday (L_3) monitored on the ^{234}U. Table 5.1 provides a summary of the combined U-Th run on the ICP MS.

Table 4.1 Typical U and Th-multi run cycle on the ICP MS

Cycle	IC_0	IC_1	L_3	IC_2	Ex-L
1	234U	233	232Th	231	230Th
2	235U	234U	233	232Th	231
3	235.5	234.5	233.5	232.5	231.5
4	236	235U	234U	233	231.5
5	236.5	233.5	234.5	233.5	232.5

U masses 233 and 234 were measured on the Faraday collector (L_3) along with Th masses 230 and 232 (L_3 & Ex-L). $^{229}Th/^{230}Th$ and U isotope ratios; $^{236}U/^{234}U$ and $^{235}U/^{233}U$ were determined from IC0, whereas $^{236}U/^{233}U$ (IC_0 & IC_2), $^{235}U/^{236}U$, $^{233}U/^{234}U$ and $^{235}U/^{234}U$ (all IC_0 & IC_1), were measured on electron multipliers. The daily variation of the ICP MS at the University of Oslo is within 2% and gain between the electron multipliers are calculated based on 235 run in IC_0 and IC_1 during cycles 2 and 3.

Gain between the Faraday and IC was measured on mass 232 (via the $^{232}Th/^{229}Th$ ratio) using a differential Tau equation. With regards to the Faraday/IC gain, the correction is invoked primarily because the Faradays do not handle rapid change in signal intensity very well. For the Th measurements, the contribution of the ^{232}Th to the ^{230}Th peak was detected by monitoring the 230 and 229 'tails'. The tail contribution refers to the influence of masses 229 and 232 on the shape of the 230 peak that is detected on the ICP MS. The mass interference is attributed to the mass similarities between these isotopes as well as the intensity of the ^{230}Th signal (Pietruszka *et al.* 2002). In this study, corrections for the Th tail are also related to the multi-static approach where the fractionation in U is used for Th. Consequently, the difference in tailing of the half masses measured on IC_0 (235.5 & 236.5) and IC_1 (234.5 & 235.5) needs to be corrected.

Approximately 1 ml of double strength $HN0_3$ was added to the evaporated eluate. Between 50 and 100 µl of this sample was then diluted in labelled test tubes using 2% HNO_3 to make *c.*5 ml. This dilute solution was used for the ICP MS analyses. An additional 100 µl of solution was added in cases where beam detection was low. Ninety repeat cycles were run for a single sample; forty cycles for uranium and fifty cycles for thorium. The ICP MS measures elements from Li to U, which covers a mass range between 5 and 250 atomic mass units (amu) (Amman 2007).

In this study, axial masses of 240.61, 241.12, 241.63 and 242.14 were used for U-series runs. For the Th runs, masses in the range from 230 to 236.5 were used. In some instances, cycles were aborted when the Th concentration was too low and could not be detected and when the ^{232}Th counts were >106. The ^{232}Th counts exceeding this threshold were taken as an indication that the collectors were being overwhelmed. The internal 'standard' (Br5), is a high U speleothem from northern Norway dated by TIMS and AMS to *c.*124 ka. A carbonate cocktail of the Br5 consisting of de-ionized water, $HNO_3$and uranium spike was used before and after a complete U-series and Th-multi run. Measuring the isotopic activity of the Br5, which has a constant ^{235}U/^{238}U ratio, was necessary to calibrate the ICP MS.

4.6 Stable isotope measurements

4.6.1 ^{13}C isotopes

Carbon has four isotopes ^{11}C, ^{12}C, ^{13}C and the radioactive ^{14}C (Fig. 4.16). The carbon isotope profile in speleothem carbonate is obtained from the ^{13}C/^{12}C ratio of dissolved inorganic carbon (DIC) species in the percolation water (*e.g.* HCO_3^-) (Ford & Williams 2007; Harmon *et al.* 2004). This isotopic ratio is determined by the soil CO_2, atmospheric CO_2 and carbonate dissolution of the limestone host

rock (Dorale *et al.* 2002; Harmon *et al.* 2004; Hendy 1971; Fig. 4.17).

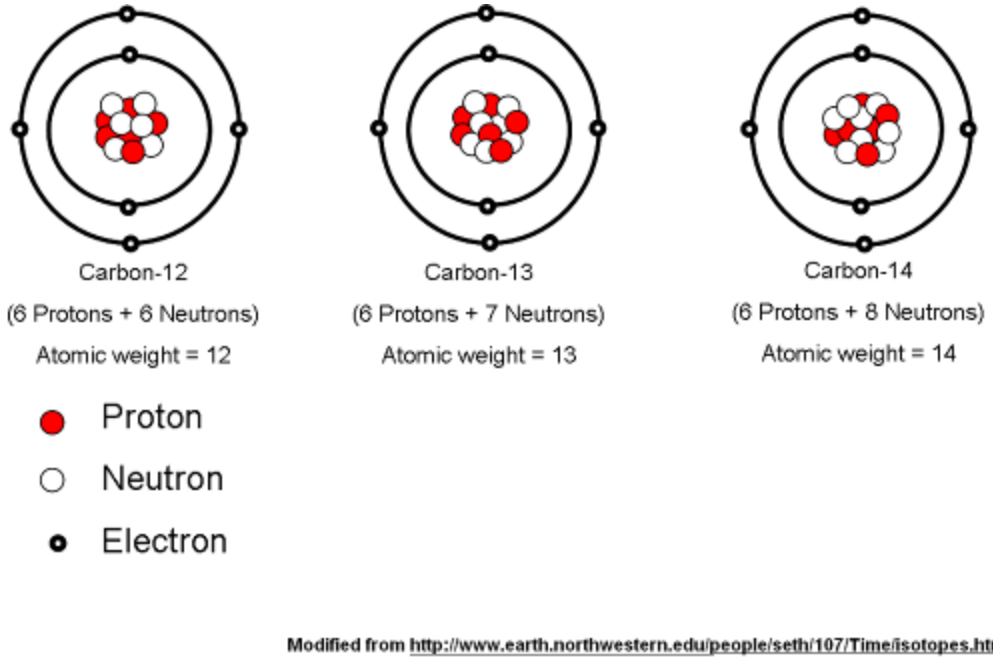

Figure 4.16 The three most abundant carbon isotopes are the stable ^{12}C and ^{13}C and the radioactive ^{14}C. These isotopes have the same number of electrons and protons within the atomic nucleus but different numbers of neutrons

The soil overlying the cave is an important source of CO_2 for carbonate dissolution. This soil-derived CO_2 is influenced by the type and extent of vegetation covering the soil and the microbial activity in the soil (Dorale *et al.* 2002; Fairchild *et al.* 2006; White 2004). Generally, the CO_2 produced during microbial decay of organic matter and photosynthetic activity is enhanced in response to rising temperatures and water availability (Ford & Williams 2007).

In speleothems, differences in the soil $^{13}C/^{12}C$ values (expressed as $\delta^{13}C$), are in turn related to vegetation above the cave. The contribution of the vegetation to the isotopic signal in the soil is linked to the different photosynthetic pathways used by plants. Trees, shrubs and temperate grasses typically use the Calvin-Benson (C_3) pathway to produce a 3-carbon phosphoglycerate compound. These C_3 plants preferentially take up the lighter ^{12}C isotope because of its affinity for the carbon fixing-enzyme Rubisco. Related to this partiality towards ^{12}C, C_3 plants have an average $\delta^{13}C$ value of -26.5 ‰. Most grasses, by contrast, use the Hatch-Slack pathway to manufacture the 4-carbon oxaloacetate compound. Plants using this pathway have an average $\delta\ ^{13}C$ value of -12.5 ‰ (van der Merwe 1982).

Plants using the Crassulacean acid metabolism (CAM) pathway such as succulents and some geophytes typically function to conserve water and because of this they are also able to switch between the C_3 and C_4 photosynthetic pathways (Raven & Johnson 1989). As a result, some CAM plants tend to have $\delta^{13}C$ values intermediate between C_3 and C_4 (van der Merwe 1982). The extent to which CAM plants utilize either C_3 or C_4 photosynthesis is usually species-specific but can also be influenced by local environmental conditions (*e.g.* temperature, rainfall seasonality & fire) (Procheş *et al.* 2006). A noteworthy feature of CAM plants is that those growing primarily under hot (& dry) conditions (*e.g.* in summer), usually have $\delta^{13}C$ values within the range of C_4 plants (Keeley & Rundel 2003). By contrast, CAM plants found in more mesic environments may have $\delta^{13}C$ values intermediate between CAM and C_3 plants (Mooney *et al.* 1977).

Although succulents are rare along the southern Cape coast the geophytes are represented fairly well with genera such as *Watsonia*, *Hypoxis*, *Cyperus* and *Bulbine* found at several archaeological sites in the region (Henshilwood 2008a). Without corresponding $\delta^{13}C$ values for these geophytes and more specifically for those using the CAM pathway (*e.g. Oxalis*), I cannot determine the contribution of CAM plants to the isotopic signal obtained from the De Hoop speleothems. Nevertheless, it is acknowledged that CAM plants may have contributed to the speleothem $\delta^{13}C$ signal (addressed in Chapter 5).

It is from the $\delta^{13}C$ signal identified in the speleothem material that broad patterns regarding the dominant vegetation above the cave may be inferred. Interpretations of the proxy signal are often focused on the contribution of C_3 and C_4 plants (Dorale *et al.* 1998). The integrity of this signal is usually preserved during carbonate deposition and changes in the isotopic values may be related to temporal shifts in the climate (White 2004; Fig. 4.17).

In glacial environments, however, where there is no soil or vegetation overlying the cave, inferring shifts in the vegetation is more complex. This is illustrated by a study at Castleguard Cave in Canada where Gascoyne & Nelson (1983) found stalagmites and soda-straws formed under the cover of ice-sheets. Based on the results from an isotopic analysis of these deposits using U-series and radiocarbon

techniques, they attributed speleothem deposition to 'incongruent dissolution of the bedrock' (Gascoyne & Nelson 1983: 540). As a result, CO_2 for speleothem deposition was derived from organic carbon residues in the bedrock. In a coastal environment such as De Hoop, where soil and vegetation is extensive, incomplete dissolution of the limestone is not likely a contributing factor in the C-isotope signal.

Variations in the ^{13}C composition of the carbonate can also be attributed to the isotopic profile of the carbonate-rich bedrock. This is because CO_2 degassing and the concomitant deposition of carbonate can occur under closed or open system conditions (Hendy 1971; Dorale *et al.* 2002; Fairchild *et al.* 2006). Under open system conditions, the percolation solution has access to a ubiquitous supply of soil CO_2 (Hendy 1971). This reservoir of atmospheric CO_2 is used to top up the aqueous CO_2 that is converted to HCO_3^- during $CaCO_3$ dissolution (Ford & Williams 2007). Consequently, the carbon precipitated from a solution under open system conditions is derived primarily from the soil (Hendy 1971). In closed system conditions, by contrast, the percolation solution only has a limited amount of CO_2, which is subsequently degassed upon entering the cave (Hendy 1971). The carbonate deposited under the closed system circumstances comprises soil carbon and carbon from the dissolution of the limestone (Hendy 1971).

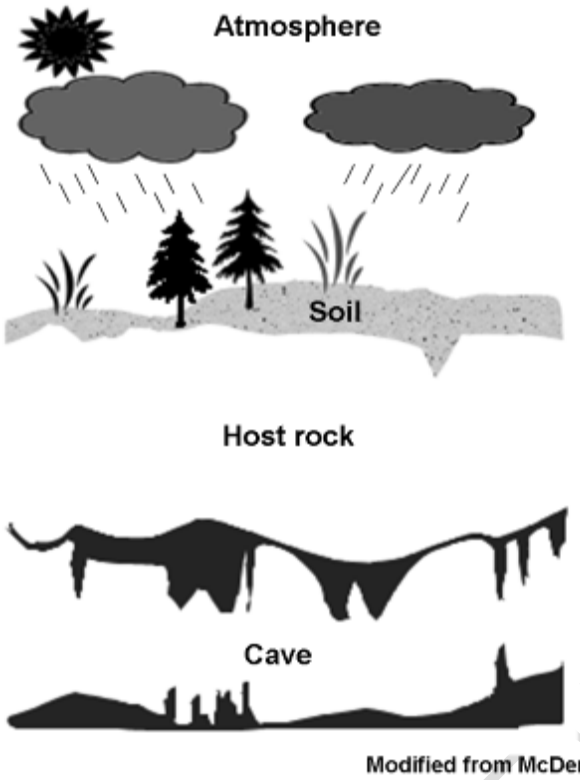

Figure 4.17 Factors above the cave that influence the speleothem isotopic signal

In addition to these effects, Baker *et al.* (1996, 1997) working at Stump Cross Caverns in Yorkshire showed that variable drip rates and the time the percolation solution takes as it meanders into the cave can have a marked influence on the enrichment of speleothem $\delta^{13}C$ values. Collectively, these processes have implications for the palaeoenvironmental interpretation of the carbon isotopes, particularly with regards to past vegetation.

In spite of the complexities associated with interpreting speleothem $\delta^{13}C$ values, general patterns do emerge. For example, under open system conditions, the C-isotopic signal is indicative of comparatively enhanced precipitation and groundwater recharge, whereas closed system conditions may reflect reduced precipitation and seasonal recharge (Harmon *et al.* 2004; McDermott *et al.* 2006). In addition, high $\delta^{13}C$ values are typically linked to cooler or drier climates in some areas but may also be related to warmer and drier conditions where changes in C_3 and C_4 plants are implicated (Harmon *et al.* 2004).

In this study, however, the existing palaeoenvironmental records (see Chapter 2) provide a useful milieu for interpreting and verifying the carbon isotope signal.

4.6.2 ^{18}O isotopes

Oxygen is the most abundant element in the earth's crust and has three stable isotopes- ^{16}O, ^{17}O and ^{18}O.

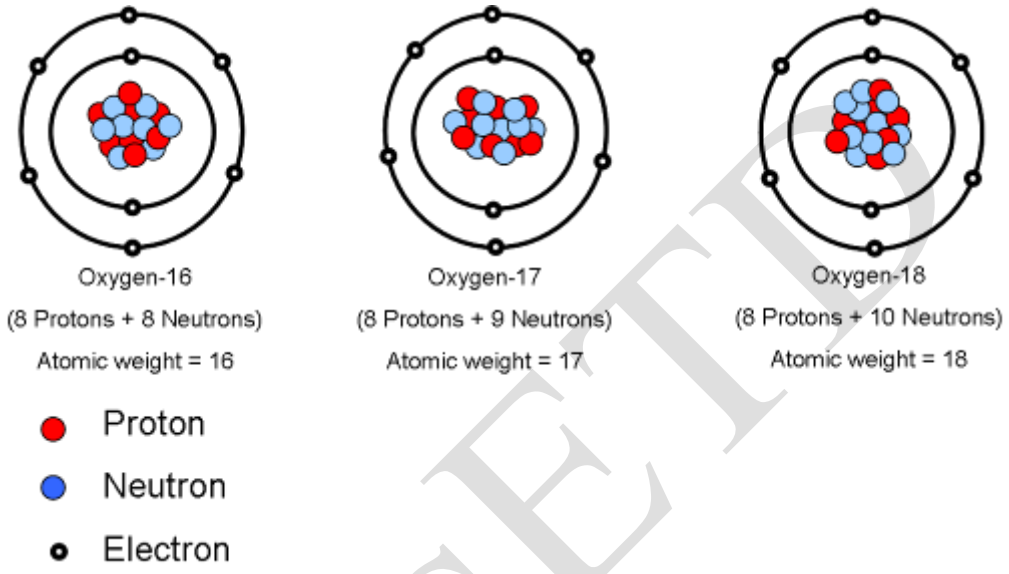

Figure 4.18 Three stable isotopes of oxygen

As a palaeoclimate proxy, variations in the $^{16}O/^{18}O$ ratio (expressed as $\delta^{18}O$), are related primarily to the percolation water (Dorale *et al.* 1998). The $\delta^{18}O$ values generally vary in response to the carbonate host rock. Limestones for example, typically have ^{18}O values > 20 ‰ whereas clastic sedimentary rocks have ^{18}O values of *c.* 20 ‰ (Hodge *et al.* 2008).

Factors operating at local, regional and temporal scales can also affect the isotopic composition of the drip water. This change in the isotopic profile of an element is known as fractionation. Fractionation refers broadly to a physical or chemical process which causes a concomitant change in the isotopic ratios of a compound (*e.g.* $CaCO_3$) or a phase (*e.g.* $H_2O_{(l)}$ vs $H_2O_{(vapour)}$). This process is quantified by comparing the isotope ratios before and after the fractionation event.

4.6.3 Fractionation & the ^{18}O signal

Isotopic fractionation is in turn related to mass differences in the atomic nuclei of the element. This mass variation causes heavier isotopes to move and react slower compared to lighter ones. Mass-linked fractionation is also known as isotopic equilibrium fractionation and occurs between two different phases of a compound (Harmon *et al.* 2004). Speleothem carbonate for example, would contain comparatively more ^{18}O than drip water CO_2. Similarly, the heavier $^{18}O^{2}H$ water is more likely to exist in the liquid phase, while the lighter $^{16}O^{1}H$ will progress towards the vapour phase (White 2004).

With regards to the stable isotopes used in this study, fractionation of carbon isotopes occurs mainly during photosynthesis. In oxygen by contrast, the $\delta^{18}O$ signal is affected by two main kinds of fractionation processes - kinetic and equilibrium effects. Of the two, the former is particularly important when interpreting the speleothem isotope signal. This is mainly because during this irreversible process, enrichment of the heavier ^{18}O isotope occurs (White 2004). Other kinetic effects influencing the oxygen isotopic ratio of the speleothem calcite are related to each step of the hydrological cycle.

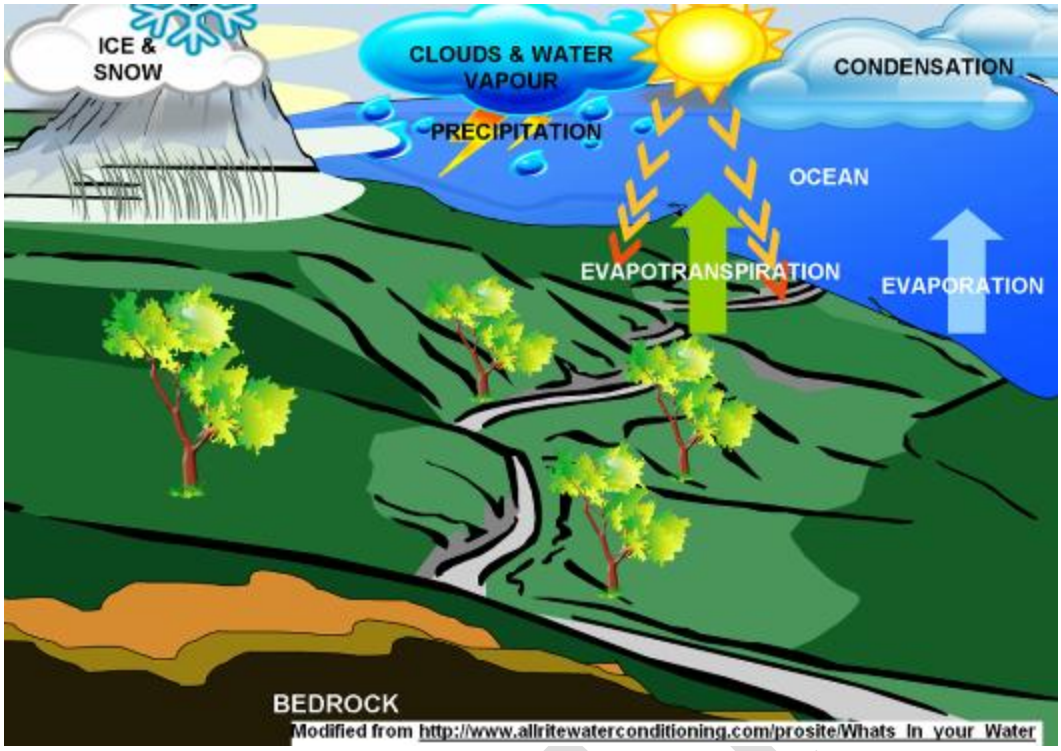

Figure 4.19 The hydrological cycle. Processes that affect the $\delta\ ^{18}O$ isotopic composition is water storage as ice and snow, precipitation, condensation, evaporation and evapotranspiration

In this cycle (Fig. 4.19), temporal variations in $\delta^{18}O$ of precipitation are largely modulated by the effects of latitude, the ocean temperature and wind (van Beynen & Febbroriello 2006). Variations in latitude are linked to the differential heating of the earth's surface. As a rule, increasing latitude reduces the angle at which solar radiation reaches the earth. Therefore, at higher latitudes where temperatures are reduced and evaporation rates are enhanced, the precipitation is generally depleted in ^{18}O.

Winds by contrast, are produced by pressure differences associated with insolation. Related to this, low-pressure systems, which typically form from warm, rising air, produce isotopically depleted precipitation. Air temperatures are also typically lower at high altitude, decreasing at a rate of *c.* 6.4 ^{o}C/1000 m. This effect is largely attributed to mountains, which force air to rise. This orographic control causes enhanced fractionation between liquid and vapour as precipitation is produced at a lower temperature (van Beynen & Febbroriello 2006). Consequently, the rain formed here is also isotopically depleted in ^{18}O.

In addition, the amount of precipitation above the cave (Gascoyne 1992; Sundqvist *et al.* 2007) and the air temperature (van Beynen & Febbroriello 2006; Sundqvist *et al.* 2007) are also contributing factors (Figs 4.19 & 4.20). These factors are related to Rayleigh distillation, which can occur during the hydrological cycle and inside the cave. In the latter, Rayleigh distillation describes kinetic isotope fractionation which occurs when CO_2 and calcite of varying isotopic compositions (compared to the rest of the DIC species in the drip water solution) are removed from solution (Wynn *et al.* 2005). This removal of gaseous CO_2 often occurs at a constant rate to maintain calcite supersaturation but leads to the enrichment of the ^{18}O isotope (Hendy 1971).

In the hydrological cycle Rayleigh fractionation can occur during condensation or evaporation of water vapour (Fairchild *et al.* 2006). This fractionation effect is determined by the amount of precipitation and is linked to the gradual depletion of the heavier ^{18}O (& ^{2}H) isotopes during rain out events (White 2004; Fig. 4.20).

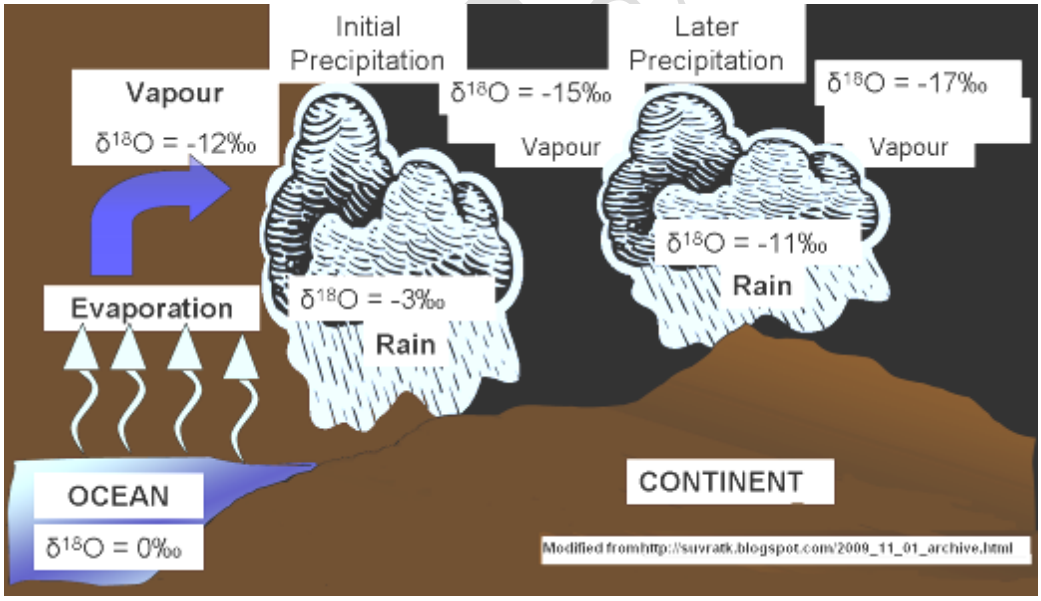

Figure 4.20 Rayleigh fractionation and the isotopic composition of precipitation during rain out events

As this ^{18}O depleted rain moves towards colder regions the remaining vapour becomes enriched in the lighter ^{16}O (White 2004). Consequently, polar ice contains more ^{16}O compared to seawater (Harmon *et al.* 2004). This Rayleigh process is represented by the following expression,

$$R = R_o \text{ x } f(\acute{\alpha}\text{-}1)$$

Where R_o is the isotope ratio prior to fractionation and R represents the altered ratio. The residual aspect is denoted as f and α is the fractionation factor (White 2004).

The contribution of these effects on the oxygen isotopic signal of precipitation is represented by the global meteoric water line;

$$\delta D = 8\delta^{18}O + 10\ (‰)\ \text{(Craig 1961: 1702)}$$

This equation illustrates the relationship between large-scale variations in the $\delta^{18}O$ composition of meteoric waters sampled from rivers, lakes, snow and rain (Fig. 4.21).

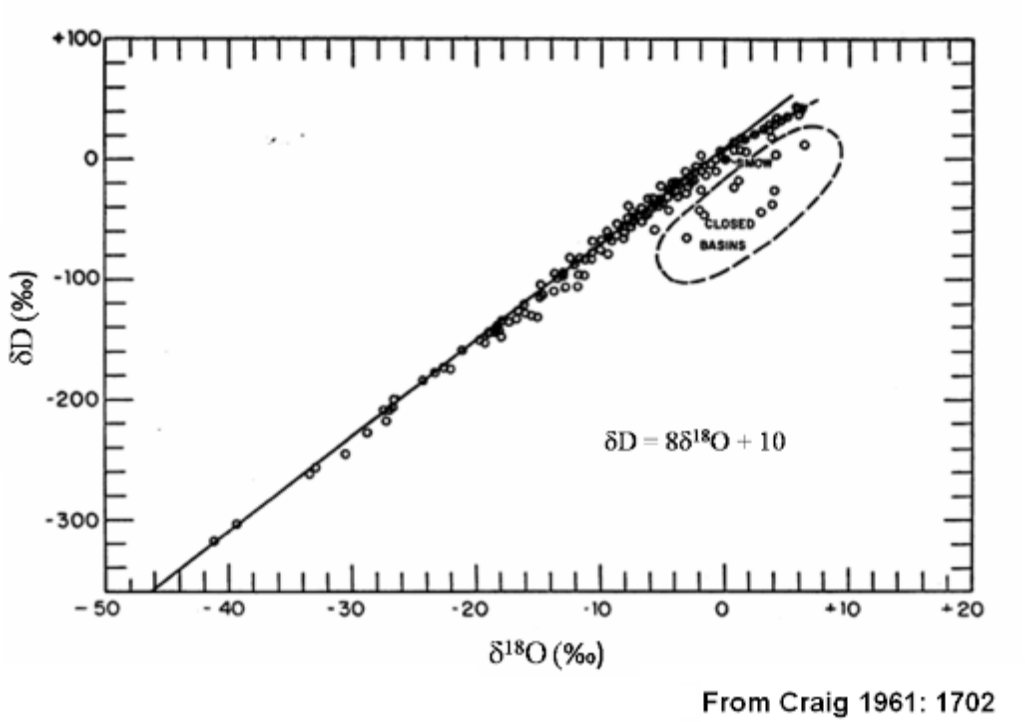

Figure4.21 Global meteoric water line (GMWL) representing the isotopic variations in water sampled from rivers, lakes, snow and rain in different regions of the world

Colder regions tend to plot at the lower end of the line while warmer regions are positioned higher up (Fig. 4.21). This is in part because of the temperature dependence of fractionation, which is reduced at higher temperatures. A consequence of this is that, precipitation formed in cool climates is often depleted in ^{18}O with the opposite effect observed in warmer climates (Craig 1961; White 2004). In these warmer regions, precipitation often becomes enriched in the heavier ^{18}O isotope at a rate of *c.* 0.5 ‰/^{o}C (White 2004).

4.6.4 Speleothem delta function (SDF) & Temperature

The $\delta^{18}O$ isotopic signal may also be connected to the temperature above the cave at the time the calcite was deposited (Fairchild *et al.* 2006; McDermott *et al.* 2006; Sundqvist *et al.* 2007). This application is however, anything but straightforward as links between the $\delta^{18}O$ signal and temperature depends on the equilibrium deposition of the speleothem calcite (Hendy 1971; Goede & Vogel 1991; Harmon *et al.* 2004).

$$\alpha_{calcite\text{-}water} = (\delta^{18}O_{calcite} + 1000) / (\delta^{18}O_{water} + 1000)$$

This fractionation factor between calcite and water ($\alpha_{calcite\text{-}water}$) is temperature dependent and consequently, it can be used to calculate the temperature at the time of deposition (White 2004).

$$\alpha_{calcite\text{-}water} = e^{(a/T)-b}$$

The temperature control on the $\delta^{18}O$ signal of the calcite and drip water was evaluated with the development of the SDF (Lauritzen & Lundberg 1999; Lauritzen & Onac 1999).

$$\delta^{18}O_{calcite} = 10^3 - [\, e\, [a/(T_1 + 237.15)]\text{-}b]]\, [F(T_2, t, g) + 10^3\,]$$

The SDF is expressed relative to VPDB. In this equation, the fractionation between calcite and water is termed the thermodynamic fractionation factor ($\alpha_{calcite\text{-}water}$) and is represented by a and b. The cave temperature is denoted by T_1 and the surface temperature by T_2 (^{o}C) although T1 ≈ T2. The drip water function, F(T,t,g), is related to the controls on precipitation in the hydrological cycle and varies temporally and geographically (Lauritzen & Onac 1999; White 2004).

These two parameters largely regulate the $\delta^{18}O$ value of the speleothem calcite (Lauritzen & Onac 1999).

The calcite-water interaction has a constant pejorative reaction to temperature, with fractionation reduced by 0.28 to 0.20 ‰/ ^{o}C (Harmon *et al.* 2004). The drip water response by contrast, varies seasonally. In terms of the SDF, these varying temperature responses are represented by μ. Where,

$$\mu. = \delta^{18}O \, (\partial/\partial T)$$

This term is used to determine which of the two parameters are dominating the calcite $\delta^{18}O$ values. Generally, when $\mu > 0$ the drip-water fractionation dominates, causing a concomitant enrichment of ^{18}O (Lauritzen & Lundberg 1999; Lauritzen & Onac 1999). The thermodynamic fractionation factor is more influential when $\mu < 0$ and leads to the progressive depletion of ^{18}O (Lauritzen & Lundberg 1999; Lauritzen & Onac 1999). On the contrary, when $\mu = 0$, the ^{18}O values remain unchanged.

Both μ and the associated drip-water fractionation can be predicted from fluid inclusions (White 2004), the meteoric water line (Craig 1961; White 2004; Harmon *et al.* 2004) and sampling of modern drips (*e.g.* Johnson *et al.* 2006). Another approach uses the temporal agreement between $\delta^{18}O$ values of coeval samples to infer equilibrium deposition and therefore a temperature-related response (Harmon *et al.* 2004).

In addition to the effects from the hydrological cycle, isotopic fractionation can also occur if water accumulates and then evaporates before entering the cave (Harmon *et al.* 2004; van Beynen & Febbroriello 2006). Air movement and low humidity within the cave (Wigley & Brown 1976; also discussed in 4.2.2) can also induce kinetic fractionation through evaporation of cave drips (van Beynen & Febbroriello 2006; Mattey *et al.* 2008). Generally, evaporation of drip water is enhanced at lower humidity (25-75%) which in turn amplifies kinetic fractionation. As an example, van Beynen and Febbroriello (2006) studying drip rate changes at Indian Oven Cave recorded fluctuations in $\delta^{18}O$ values at different locations within the cave. Related to this, the authors noted that at one such

location, enriched summer ^{18}O values were reflected in the cave drips during winter. At this particular entry point, flow ceased during winter. Consequently, calcite was deposited primarily from summer drips. The implication of this observation is that variations in the $\delta^{18}O$ signal may not necessarily be indicative of palaeoclimatic change.

Understanding the interplay between these various parameters is therefore particularly important when relating isotopic changes to specific periods of climatic change (McDermott *et al.* 2006).

4.7 Sampling for the stable carbon and oxygen isotope analyses

4.7.1 Sampling for stable C and O isotope analyses

Subsamples for stable isotopic analyses were taken from the central axis along the growth (deposition) layers of stalagmite material at 5-10 mm intervals using a dentist drill with a 0.5 mm burr tip. Isotope measurements were obtained from four speleothems representing Bloukrantz Cave (*Blou1*) and Kaisers Gat II (*KG2.1*, *KG2.2* & *KG2.3*). Supplemental samples were also taken along the growth layers of the stalagmites (& flowstones) from these caves. This was done by drawing a line down the length of the stalagmite and drilling from the top of the sample material to the base at 0.5-3 mm intervals on either side of the line (Fig. 4.22). This strategy would provide a general view of the isotopic signature for the region, help reduce sample averaging and identify discrepant isotopic values (*e.g.* Constantin *et al.* 2007).

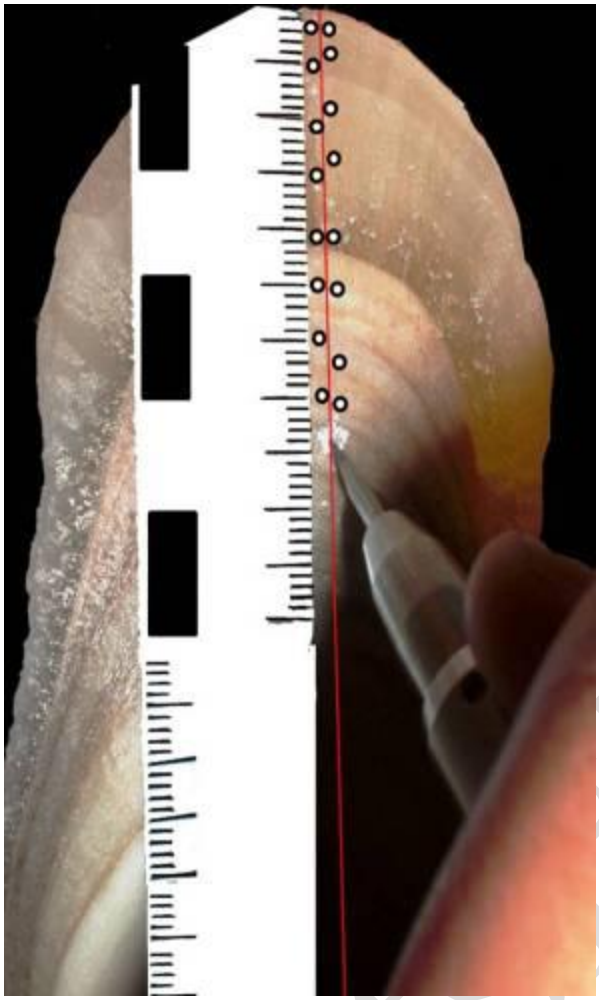

Figure 4.22 Sub-sampling approach used for the stable isotope measurements with samples taken on either side of the vertical line between 0.5 and 3mm intervals from the top of the stalagmite (or flowstone) to the base

The powdered sample material was collected on A5-sized wax-free paper, weighed and transferred into small, dry glass vials before loading into a sample carousel. Each vial contained between 60 and 100 µg of sample. The drill bit, drilling area and balance were cleaned after each sample was taken.

Isotopic ratios for $^{13}C/^{12}C$ and $^{18}O/^{16}O$ were measured on a dual inlet Finnigan™ MAT 253 at the Bjerknes Centre for Climate Research at the University of Bergen. A mass spectrometer essentially ionizes molecules and separates them according to their mass-to-charge ratio. With an isotope ratio mass spectrometer such as the MAT 253, the ions are measured simultaneously on a series of Faraday collectors. This data is then evaluated using the operating Isodat software. The main components of a mass spectrometer are the inlet system, ion source,

accelerator or flight tube, an analyser and the detector. A schematic of the MAT 253 is represented in Figure 4.23.

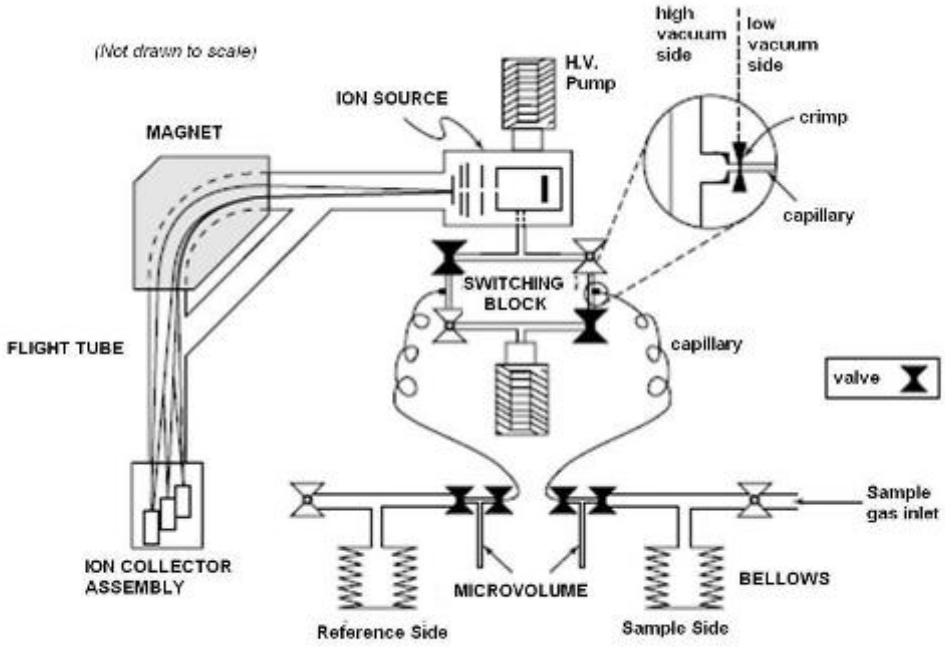

Figure 4.23 Diagram of the MAT 253 mass spectrometer showing the series of valves, vacuums and capillaries, which direct the movement of the sample and reference gas from the inlet system to the switching block. Ionisation occurs at the ion source and from there the ions are accelerated down a flight tube and eventually measured at the detector

The dual inlet system of the MAT 253 tolerates pure gases of CO_2, H_2, N_2 as well as O_2. In this study, the powdered sample material was fed into a carbonate device connected to the inlet system. It was here that the CO_2 gas needed for the analysis was liberated from the sample. The carbonate device consists of an autosampler carousel, a series of valves and vacuums, two traps and a phosphoric acid reservoir (Fig. 4.24).

In this study, the autosampler carousel containing *c.* 40 sample vials and 8 vials with laboratory standard was connected to the carbonate-device chamber of the mass spectrometer. Here it was sealed inside a vacuum at 61 atm to remove the CO_2 (g). The samples were dissolved in three drops of concentrated phosphoric acid (H_3PO_4) (maintained between 65.5 ^{o}C & 70 ^{o}C) using the dual inlet system of

the MAT 253. At this temperature $CaCO_3$(s) is fairly stable and this reduces phase change related fractionation. The reaction between the solid carbonate sample and H_3PO_4 is shown in the equation below:

$$H_3PO_4(aq) + CaCO_3(s) = H_2O(g) + CO_2(g)$$

The CO_2 and H_2O produced during the reaction above were separated by first freezing the gases on liquid nitrogen at -170 ^oC and warming the reaction products to -120 ^oC to liberate the CO_2, which was then pumped into a second chamber and cooled to -170 ^oC. This process is illustrated in Figure 4.24.

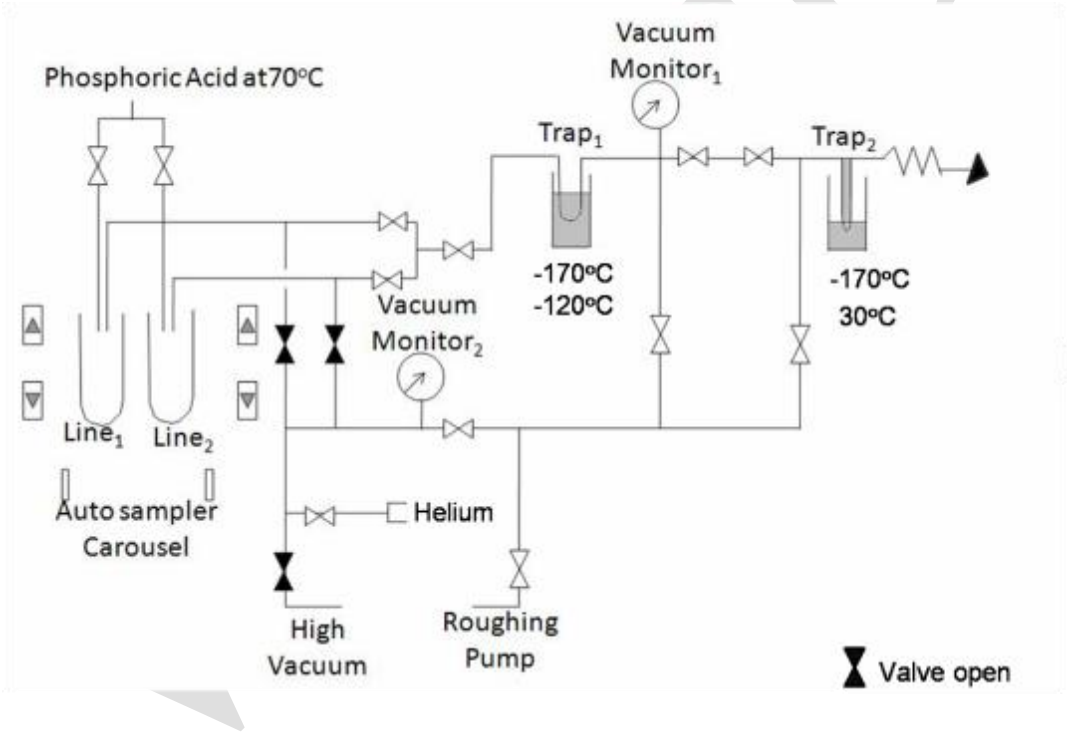

Figure 4.24 Schematic of the main components of the MAT 253 Kiel carbonate device showing the autosampler carousel, the phosphoric reservoir, vacuum pumps and valves. At traps 1 and 2 the gaseous CO_2 and H_2O liberated during the reaction of the carbonate sample with phosphoric acid (H_3PO_4) are separated

The duration of the first reaction is close to 470 s and any non-condensable gases were pumped away for 30 s inside a waste vacuum line. Warming trap 1 to -120 ^oC liberated the CO_2 as a gas while keeping the water frozen. The CO_2 was pumped via the connection valves to trap 2 and cooled to -170 ^oC. As a result of this cooling the products from trap 1 and 2 were separated. Warming the frozen

gas in trap 2 to *c.* 30 ^{o}C resulted in the gas being transferred via a capillary tube connected to the changeover valve to the inlet system of the mass spectrometer. The inlet system consists of a series of valves, pipes, capillaries and vacuum gauges with the changeover valve forming the core. It is here that rapid exchange, usually within seconds, between the reference and sample gases takes place. Gases are pumped from the bellows (sample & reference gas stores) to the changeover valve (or switching block). The viscous flow of the gases through the capillaries (0.1-0.2 mm) is maintained at 15 mbar by adjusting the crimps to direct and control the movement of the gases. This is achieved when one gas enters the inlet system and the other gas is moved towards the waste pump where it is removed. From the inlet system, the gaseous sample enters the ion source where the following reaction occurs:

$$CO_2\ (g) + e^- \rightarrow CO_2^{2+} + 2e^-$$

The reaction occurs because electrons emitted by the tungsten filament in the ion source collide with the CO_2 gas molecules to produce CO^{2+}ions. These ions (*i.e.* CO^{2+}) form through a complex series of reaction pathways during which C^+, O^{2+} and CO^+ ions are produced (Zavilopulo *et al.* 2005).

The newly formed CO_2^+ions are then accelerated at *c.* 10 kV under the influence of an electromagnet towards the detector. In this study, the data was analysed using the Isodat operating software and expressed in delta notation relative to the Cretaceous belemnite *Belemnitella americana* from the Peedee formation in South Carolina known as PDB. Before it was used up, PDB was the original international standard for carbon isotopes:

$$\delta^n X\ (\text{in } ‰) = 1000\ [(R_{sample}/R_{standard}) - 1]$$

Where n is the rare isotope of the element, represented by the symbol X and R is the isotope ratio.

Another limestone - NBS20 – scaled relative to PDB (-1.06 ‰) was used as an alternative. It was subsequently replaced by NBS19 and defined as V-PDB

(Vienna PDB). V-PDB has an isotopic composition of 0.011 for $\delta^{13}C$ and 0.002 for $\delta^{18}O$.

V-SMOW (Vienna Standard Mean Ocean Water) is 0 for $\delta^{18}O$ and is the international standard for oxygen isotopes. The $\delta^{18}O$ values may be reported relative to two standards; one for water samples (V-SMOW) and one for carbonates (V-PDB). This is primarily because isotopic measurements on water and carbonates are derived from gaseous CO_2 that is either reacted with or produced from the sample. The relationship between V-SMOW and V-PDB is expressed in the following equation:

$$\delta^{18}O_{V\text{-}SMOW} = 1.03091 \times \delta^{18}O_{V\text{-}PDB} + 30.91 \text{ ‰}$$

In this study, $\delta\ ^{18}O$ and $\delta^{13}C$ obtained from the carbonate samples are reported relative to V-PDB.

At the Bjerknes Centre Carrara marble (CM03) is used as a secondary reference material along with NBS-18. This is a common practice at isotope laboratories as there is only a limited amount of the standard available for analyses. However, isotope ratios obtained on a secondary reference material have to be calibrated with the standard before being reported. This is generally done using the following equation:

$$\delta\ (Sa/St) = \delta\ (Sa/Ws) + \delta\ (Ws/St) + 10^{-3}\ [\delta\ (Sa/Ws) + \delta\ (Ws/St)]$$

Where WS denotes the 'in-house' standard, St represents the international standard (*e.g.* V-PDB or V-SMOW) and Sa is the measured sample (Brand 2004). The reproducibility of 'in-house' standards on the Bjerknes Centre MAT 253 is within 0.1 ‰ for ^{18}O and 0.05 ‰ for ^{13}C. Ratios were also corrected for isobaric interference, background, linearity and to a lesser extent for memory effects. Isobaric interference refers to the influence of ion currents generated in the Faraday cups by ions other than those being analysed (Brand 2004). As an example, CO_2 exists in the form of $^{44}CO_2$ (as $^{16}O^{12}C^{16}O$); $^{45}CO_2$ ($^{16}O^{13}C^{16}O$ & $^{17}O^{12}C^{16}O$) and $^{46}CO_2$ (as $^{18}O^{12}C^{16}O$). The ^{13}C signal is determined from the 45/44 mass ratio with ^{12}C obtained from mass 44 and ^{13}C from mass 45. For the oxygen

signal there is interference from ^{17}O on mass 45. This is corrected for using the Craig equation, which is automatically invoked using the Isodat software. The Craig equation is expressed mathematically as:

$$\delta^{13}C = 1.067645\delta_{meas} - 0.0338\delta^{18}O$$

The 'background' is attributed to a residual signal and is measured when there is no gas in the mass spectrometer (Brand 2004). This measurement is accounted for automatically with the aid of the operating software. Memory effects are related to sample mixing and may occur when samples are reacted in a common acid vessel (Brand 2004). This may be an important consideration since phosphoric acid was added to each of the samples via the acid drip valve.

In this study, the influence of memory effects was reduced by cleaning the tip of the acid drip valve and adjacent rubbers before and after each run. Linearity, in contrast, refers to mixing between the sample and reference gases that may occur at the changeover valve during a period known as the residence time (Brand 2004). At the Bjerknes Centre, non-linearity is monitored by evaluating the activity of the in-house standards; NBS-18, CM03 and the reference gas.

Graphical representations of the stable isotope and U-series data are presented in Chapter 6 and were generated using DPlot Jr. Software and Microsoft Excel.

4.8 Summary

Speleothems are secondary cave deposits that form when rain absorbs atmospheric CO_2 from the air and the soil, thereby producing carbonic acid for limestone dissolution. Once this percolation solution reaches an air-filled cave the CO_2 is degassed and dissolved minerals suspended in the solution consequently precipitate out. The progressive build-up of the precipitates on different sections of the cave eventually produces stalagmites, stalactites and flowstones.

The speleothems used in this study were obtained from selected caves in the De Hoop Nature Reserve on the South African south coast. The stable carbon and

oxygen isotope records preserved in the sampled stalagmites and flowstone deposits were used as proxy indicators of vegetation and rainfall, respectively. Temporal constraint for the speleothem-derived palaeo-data was obtained using uranium series dating based on the $^{230}Th/^{234}U$ disequilibrium method with an age range up to 350 ka.

Relating changes in the isotopic ratios to specific climatic parameters is complex. This is because the photosynthetic pathway of the vegetation influences changes in the carbon isotope ratios while variations in the oxygen isotopic signal are mainly affected by rainfall seasonality and temperature. The reliability of the isotope values recorded on the speleothem samples were therefore evaluated using a replication approach, which is based on concordant isotope profiles.